COASTAL HAZARD ANALYSIS AT SAN ONOFRE NUCLEAR GENERATING STATION

Part 2: Geological Hazards



for

SOUTHERN CALIFORNIA EDISON
P.O. Box 128, MS D3D
5000 Pacific Coast Highway
San Clemente, CA 92672

Coastal Environments, Inc.
2166 Avenida de la Playa, Suite E
La Jolla, CA 92037

CE Reference No. 22-03
31 March 2022

TABLE OF CONTENTS

EXECUTIVE SUMMARY iii

1.0 INTRODUCTION 1

2.0 SEISMIC HAZARDS 3
2.1 BACKGROUND – REGIONAL TECTONIC DEFORMATION 3
2.2 GROUND SHAKING HAZARDS 12
2.2.1 Seismogenic Faults 12
2.2.2 Probabilistic Seismic Hazard Assessment 13
2.2.3 Methods of the GeoPentech 2010 PSHA 15
2.2.4 Seismic Sources 16
2.2.5 Seismic Risk 18
2.2.6 Coastal Fault System 20
2.2.7 Hypothetical M_W7.6 Scenario Earthquake 23
2.3 GROUND FAILURE HAZARDS 27
2.3.1 Surface Rupture 27
2.3.2 Liquefaction 27
2.3.3 Slope Stability 28
2.3.4 Bearing Capacity 31

3.0 REFERENCES 32

LIST OF APPENDICES

Appendix A. SONGS ISFSI Slope Stability A-1
Appendix B. ISFSI Foundation Design B-1

LIST OF FIGURES

Figure 2-1. Map of complex geologic structure of Pacific-North America tectonic plate boundary 4
Figure 2-2. Potential seismic source map with updated UCERF3 faults in orange, and upper tips of detachments, black with hashes in dip direction 8
Figure 2-3. Southwest California historic earthquakes, 1850-2008 are Seismicity cross-sections with 15-mile wide buffers 9
Figure 2-4. SONGS with 1981-2019 magnitude M>2 relocated earthquake positions 10
Figure 2-5. Earthquake swath profiles across the Inner Borderland offshore San Onofre 11
Figure 2-6. Thickness of late Quaternary sediments in the Inner Borderland between Dana Point and La Jolla 17
Figure 2-7. Comparison of hazard curves 2010 PSHA and 1995 PSHA 19
Figure 2-8. Map and photograph of paleoliquefaction sites exposed in a cut slope along Encinas Creek, Carlsbad 22
Figure 2-9. Photograph of paleo-earthquake fault rupture with liquefaction sand deposits covering 40,000-yr soil and fault scarp 22

Figure 2-10. Map of simplified fault rupture model for M_W7.6 earthquake along the Coastal Fault System.....25
Figure 2-11. High-resolution 24-channel seismic profile of Newport-Inglewood fault uplift that blocks Quaternary paleochannels offshore Oceanside.....26
Figure 2-12. Plan view of West UMAX and NUHOMS ISFSIs.....30

EXECUTIVE SUMMARY

The coast of southern California lies within the active tectonic plate boundary between the oceanic Pacific plate and the continental North America plate. The San Andreas fault system represents the major strike-slip transform fault along this boundary, but tectonic deformation and complex fault zones cover a broad area across the Continental Borderland and Peninsular Ranges relevant to the San Onofre Nuclear Generating Station (SONGS). Geological hazards analyzed for the SONGS NUHOMS Independent Spent Fuel Storage Installation (ISFSI) include seismic hazards associated with earthquakes, ground failure, surface rupture, liquefaction, slope stability, and bearing capacity.

Background Studies

Decades of geological research sponsored by Southern California Edison (SCE) in the SONGS area have provided a good understanding of the active deformation of this complex region to assist in safe design and construction of facilities at SONGS, including the NUHOMS ISFSI. These investigations recognized the right-lateral Newport-Inglewood-Rose Canyon (NIRC) strike-slip fault zones as critical features that control the earthquake hazard at SONGS. The Design Basis Earthquake DBE for SONGS was set at 0.67g (gravitational acceleration). This estimate was based on a 7.0 magnitude earthquake.

The Oceanside blind thrust low-angle fault system (OBT) shows deformation characteristic of strain reversal, proceeding from prior extension to present-day contraction with blind thrust faulting. Seismic hazard assessments based on the strike-slip faulting of the NIRC were adjusted to include the potential for large blind thrust earthquakes, similar to events observed elsewhere in California (GeoPentech, 2010).

SCE in conjunction with scientists at the Southern California Earthquake Center (SCEC) worked together to develop a more comprehensive earthquake hazard model with the numerous active faults mapped in the past 10-15 years. The Unified California Earthquake Rupture Forecast, version 2 (UCERF2), was the basis for the report provided by GeoPentech (2010). The research continued as SCE held several workshops from 2011 to 2013 and SCEC updated the comprehensive model to UCERF3 to specifically address the multi-fault rupture earthquakes.

Probabilistic seismic hazard assessments (PSHAs), based on the early models, predicted substantially more moderate (M5.5-6.5) earthquakes than were recorded in the seismicity records. Increasing the maximum magnitudes in the model afforded by multi-fault rupture scenarios produced better agreement with the historical earthquake records. With fewer moderate, but relatively frequent earthquakes in the model, the expected peak ground acceleration (PGA) values dropped from 0.31g for the NIRC to about 0.23g at the 475-yr return period (10% exceedance in 50 years). Consequently, the 1.5g design value remains conservative for shaking hazard at the ISFSI.

Recent Work

In the past decade, additional large complex earthquakes struck, including the 2014 MW7.2 El Mayor-Cucapah (Baja California) and MW7.8 Kaikōura (New Zealand) earthquakes that involved combinations of strike-slip and low-angle faults (detachments and subduction thrusts) that produced extreme levels of deformation and strong ground motions. The complex fault rupture pattern of the Kaikōura earthquake resembles the complex faulting in the Coastal Fault System, dominated by the strike-slip NIRC and including the San Mateo, San Onofre, and Carlsbad faults all underlain by the OBT and Thirtymile Bank Detachment.

In 2022, Coastal Environments analyzed a large hypothetical 7.6 magnitude earthquake model at SCE's request to evaluate the worst-case seismic hazards at SONGS. The hypothetical modeled earthquake exceeds previous maximum magnitude events (M7.0-7.3) considered for SONGS design and could produce greater damage, including tsunami inundation. However, the large magnitude events are extremely rare, with return periods estimated at about 10,000 years. This exceeds the 7,143 year recurrence of the Design Basis Earthquake (DBE) for SONGS Units 2 and 3, having a peak ground acceleration of 0.67g. For the design of the NUHOMS ISFSI in 2001, a much higher 1.5g peak ground acceleration (considerably higher than the NRC-approved SONGS DBE criteria) was selected to ensure that seismic design basis did not underestimate the seismic risk at the site. Consequently, the existing 1.5g peak ground acceleration established for the ISFSI design remains conservative for the seismic hazards identified for the SONGS site, even in light of new modeling that accounts for recent earthquake information.

With respect to liquefaction hazards, the SONGS ISFSIs are built on dense, well-consolidated sands of the San Mateo Formation, which extend about 900 feet below the ISFSI site (SCE, 1995; GEI, 2015), and are considered to be at low risk of seismically-induced liquefaction. Ground water measurements at the ISFSI site were at elevation 5.03 ft. MLLW in 2020, or about 14.72 feet below the NUHOMS concrete support pad. Even under the extreme hypothetical H++ sea level scenario (+2.80 ft MSLR by 2050), groundwater under the ISFSI site is still projected to remain about 11.92 feet below the NUHOMS ISFSI support pad and will not affect the previous Coastal Commission findings that subgrade under the support pad is stable with respect to bearing capacity and liquefaction.

With respect to slope instability, the slopes north of the NUHOMS ISFSI are about 105 feet away from the ISFSI's spent fuel canisters. Hinkle (2007) found that when conservatively assuming a slope failure during a design seismic or a tsunami event, the anticipated slope run-out distance of the adjacent slope is about 91 ft. Therefore, any slope failures from the north bluff would not result in run-out that comes closer than about 15 feet away from the ISFSI. Accordingly, the previous findings by the Coastal Commission related to stability of the slopes adjacent to the NUHOMS ISFSI and potential effects on the project remain valid.

As part of this analysis, Coastal Environments has reviewed the 2001 and 2015 SONGS ISFSI Coastal Development Permit (CDP) and staff report materials and found that the Coastal Commission's conclusions in those reports remain correct.

COASTAL HAZARD ANALYSIS AT SAN ONOFRE NUCLEAR GENERATING STATION

Part 2: Geological Hazards

1.0 INTRODUCTION

The objective of this study is to update the seismic hazard analysis for the San Onofre Nuclear Generating Station (SONGS) and to evaluate the most recent current available geologic, seismic, and ground motion information in the vicinity of SONGS to determine their impacts on the NUHOMS Independent Spent Fuel Storage Installation (ISFSI). We have reviewed newly published reports, papers, and data regarding geological, geophysical, and seismic hazards along the coast of southern California.

SONGS is located on an elevated coastal plain in San Diego County, California, about 18 km south of Dana Point and 24 km north of Oceanside. The site is adjacent to the north end of San Onofre State Beach at the northwest corner of Marine Corps Base Camp Pendleton (MCBCP). The ISFSI is located in the North Industrial Area (NIA) where the decommissioned SONGS Unit 1 was located before its deconstruction in 1999. The ISFSI is constructed on a pad cut into the former Pleistocene marine terrace deposits and underlying Pliocene San Mateo Formation of marine sandstone and conglomerate beds. The ISFSI is planned to store spent nuclear fuel until 2050, by which time the U.S. Department of Energy (DOE) is expected to take custody of the spent fuel for permanent storage at as yet an undetermined location.

In this report, we review the advancements in understanding of active faulting that determine earthquake potential at San Onofre. Changes in seismic hazard estimates over the past two decades are discussed, and new information presented and compared with previous studies. According to the California Coastal Commission staff report (CCC, 2001), "*Within Southern California Edison's proposed 35-year timeframe, the siting and design of the ISFSI would be sufficient to assure stability and structural integrity against geologic hazards …, without requiring shoreline protection.*"

Geological hazards at the ISFSI include earthquake hazards, slope movement or failures (landslides) along the coastal bluffs and inland natural and cut slopes, coastal erosion, sea level rise, and coastal flooding from storm surge or tsunami. Seismic hazards are discussed in Chapter 2. These hazards include earthquake fault rupture, strong ground motion (shaking), and secondary ground failures – liquefaction, landslide, and tectonic fractures such as tectonic uplift or subsidence.

Regional tectonic deformation is described in Section 2.1. An important observation is that the Pacific plate has always been moving away from the North America plate in California, resulting in a highly complex network of faults and extensional rifts along the continental margin, both on land and offshore. In addition, the San Andreas fault system and the California Continental Borderland also include numerous strike-slip and extensional "normal" faults.

Section 2.2 discusses ground shaking hazards. Ground shaking is dependent on earthquake magnitude, distance from the fault rupture and its direction of propagation, and soil conditions. Secondary ground failures, including liquefaction of susceptible materials, or slope failures could be induced in areas of strong shaking. Evaluating these hazards probabilistically depends on characterizing the processes that produce these risks, including seismogenic faults and their sources.

In Sections 2.2.5 and 2.2.6, we discuss seismic risk and the Coastal Fault System in the vicinity of San Onofre. New research has increased the likelihood estimation of large (M>7) magnitude earthquakes and determined these to be, on average, 10,000-year events. Simultaneously, this work has shown that moderate quakes (M5-7) are less frequent to occur than previously thought.

Section 2.3 concerns seismic ground failure, summarizing surface rupture and liquefaction risks, and slope stability and bearing capacity relevant to the SONGS ISFSI. We determine that large, but low probability multi-fault earthquakes may produce subsurface fractures, but that the rigid ISFSI construction will reduce impacts from such effects. We also show that horizontal and vertical shaking is within the original design parameters of the ISFSI. Additionally, the nearest slopes are sufficiently distant to pose no direct hazard, and that the underlying bearing capacity is more than sufficient to support the ISFSI as designed.

Chapter 3 presents an extensive list of references cited in this study, including pertinent papers published from 2015-2021.

2.0 SEISMIC HAZARDS

SONGS is located along the coast of southern California between Dana Point and Oceanside on the northwest end of MCBCP. Seismic hazards that may affect the ISFSI at SONGS include earthquake fault rupture, strong ground motion (shaking), and secondary ground failures – liquefaction, landslide, and non-tectonic fractures. In addition, tsunami induced by tectonic or landslide deformation offshore in the adjacent California Continental Borderland or from tectonic or volcanic activity around the Pacific "Ring-of-Fire" may be destructive to coastal structures. Tsunami hazards are discussed further in Part III Tsunami Hazards.

2.1 BACKGROUND – REGIONAL TECTONIC DEFORMATION

Earthquakes are the result of tectonic deformation, which can create major geographic features including mountain ranges or ocean basins. In southern California, tectonic deformation is controlled by the Pacific-North America transform fault plate boundary and faults of the San Andreas fault system (Atwater, 1970; Lonsdale, 1991; Atwater and Stock, 1998). The crust along the western edge of North America has been sliced by many faults that were active during different time periods of the plate boundary evolution. The former trench at the Patton Escarpment was the major subduction shear zone where the ancient Farallon oceanic plate was thrust beneath the North American continent. Broad-scale overview of these features and relative plate motions is illustrated in Figure 2-1.

About 30 million years ago, the East Pacific Rise seafloor spreading center reached the edge of North America. This seafloor spreading ridge was segmented in a zig-zag configuration with extensional rifts separated by oceanic transform faults. The resulting strike-slip transform fault interaction with the North American continent grew outward with the Mendocino transform fault triple junction moving to the north past San Francisco and the Rivero extensional rift triple junction moving south past Baja California. Some blocks of ancient Farallon oceanic crust were captured as microplates (Nicholson *et al.*, 1994) along with the western edge of North America continental crust to join the Pacific Plate on its northwest trek towards Alaska.

An important observation is that the Pacific Plate has always been moving away from the North American continental margin in California. The resulting complex network of faults includes strike-slip and extensional rift zones created along the continental margin above the former subduction mega-thrust as the San Andreas transform fault system evolved. The California Continental Borderland formed as a major rift area that includes numerous strike-slip faults in addition to the extensional "normal" faults.

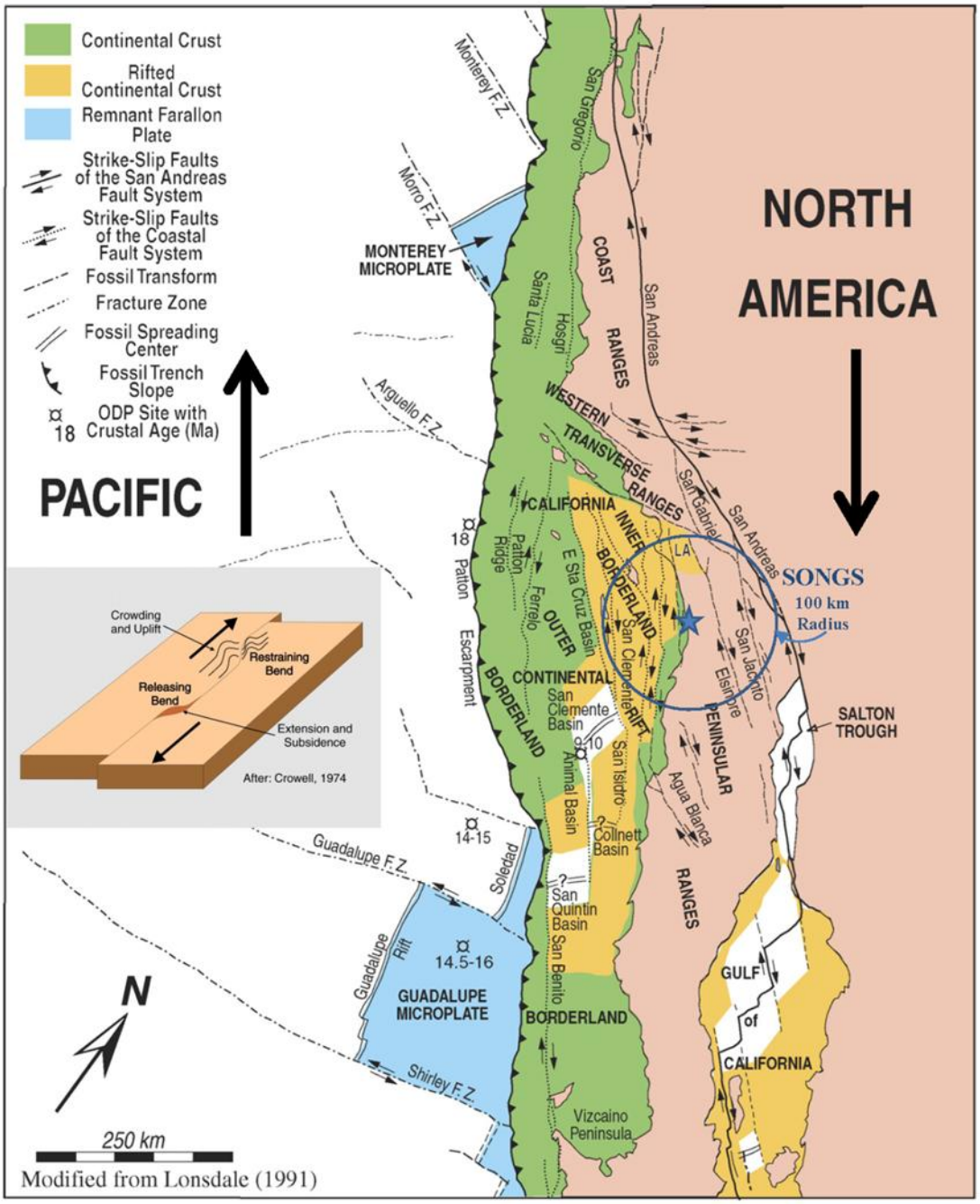


Figure 2-1. Map of complex geologic structure of Pacific-North America tectonic plate boundary (green and yellow areas are offshore). San Onofre near middle of broad shear zone accommodating Pacific-North America relative plate motion.

The San Andreas and other major northwest-trending faults along the plate boundary are right-lateral strike-slip faults that accommodate the northwest translation of the Pacific oceanic plate relative to the North America continental plate. Complications in the geometry and rheology (mechanical properties) of the crust along the plate boundary produce zones of oblique-deformation where combinations of horizontal strike-slip and vertical displacements occur on faults with varying orientations. Fault surfaces with strike or dip directions that deviate from the predominant northwest-trending vertical strike-slip fault surfaces produce oblique-deformation. In particular, a major westward bend of the San Andreas fault zone in southern California creates a restraining fault geometry where crustal material converges and produces vertical deformation (Crowell, 1974).

Uplift of the Transverse Ranges and down-welling of crustal material into the mantle produce crustal thickening to accommodate the horizontal shortening. The strike-slip faults of the region have numerous restraining bends, where convergence produces crustal uplift (transpression), and releasing bends or stepovers, where divergence, produces crustal subsidence (transtension, Figure 2-1).

The complex deformation is evident offshore where the former subduction zone was replaced by a Miocene oblique-rift – the Inner Borderland located between the fault zone west of San Clemente Island and the coast (Moore, 1969; Legg, 1991; Crouch and Suppe, 1993; Bohannon and Geist, 1998). The collision of the Inner Borderland with the Western Transverse Ranges enhances the oblique-slip with transpression offshore southern California (Sorlien *et al.*, 2016) whereas transtension persists offshore northwest Baja California (Legg, 1985; 1991; Legg *et al.*, 1991). Within the continent to the east, the Salton Trough and Gulf of California maintain a system of right-lateral transform faults that link nascent and growing seafloor spreading centers (Lonsdale, 1991) to accommodate the northwest translation of the Baja California and Borderland microplates along with the Pacific oceanic crust.

Other important active right-slip faults, with northwest trends parallel to the Pacific-North America relative plate motion, include the San Jacinto and Elsinore faults onshore, and the San Clemente and San Diego Trough faults offshore illustrated in Figure 2-2. The GeoPentech's (2010) report's Figure 3-7 has been modified to include a subsequent update (#3) of the Unified California Earthquake Risk Forecast (UCERF3, 2013)[1]. Although SONGS is located near the center of the broad Pacific-North America transform plate boundary, it lies on the edge of a relatively stable crustal block consisting of the Peninsular Range granitic crust with the nearest Type A[2] fault located 22 miles northeast across the Santa Margarita and Elsinore Mountains.

The faults along the San Andreas transform fault system are numerous and sustain widely-varying geometry and slip character. Although most of the active strike-slip faults are vertical, the dip-slip and oblique-slip faults have dips that span the full range from vertical to nearly horizontal, including nearly flat-lying detachments associated with Miocene rifting,

[1] UCERF updates are numbered.

[2] Type A, B, and C faults are USGS and California Geological Survey definitions. A=very active and well-defined, slip rate >5 m/yr; B=active and well-defined but slower or unknown slip rate; C=faults that are known or thought to exist, but have poor data to define their traces or activity, which includes many offshore faults.

roughly 10-20 million years ago (Ma). Consequently, the character of deformation and earthquake potential affecting the SONGS site is complicated. The distribution of historic earthquake sequences provides a direct indication of where active faulting exists (Figure 2-3). Faults located within 60 miles of the site are considered in this seismic hazard assessment.

Additional faults have been identified and mapped since the 2010 analysis, including steep strike-slip and reverse faults (Figure 2-3, orange), as well as the low-angle detachments that may be reactivated as blind thrust faults (gray with hachures). Historic earthquakes show that the fault activity is clustered along major faults, but also includes widespread events located between mapped faults. In areas of convergence, including the Transverse Ranges, blind thrust faults produce broad aftershock distributions where no surface faults are mapped, as for example during the 1994 M_W6.7 Northridge earthquake (Teng and Aki, 1996). Relocation of seismicity using advanced methods (waveform cross-correlation) and 3D seismic velocity models provides a more accurate representation of active faulting below the surface (Figure 2-4).

Decades of careful research have compiled reasonably accurate descriptions of the hazard potential in the San Onofre region (e.g., GeoPentech, 2010). Hazard estimates are updated as results from new research unearth additional details of the complex tectonic environment.

Black lines (Figure 2-4) show locations of a portion of the exploration industry seismic profiles available through the U.S. Geological Survey USGS NAMSS database (Treizenberg *et al.*, 2016). The 1933 M_W6.3 Long Beach earthquake ruptured the mapped Newport-Inglewood-Rose Canyon (NIRC) fault zone (Hauksson and Gross, 1991) In contrast, the offshore 1986 M_S5.8 Oceanside earthquake involved a complex zone of subseafloor faults that included a low-angle detachment "blind thrust" (Hauksson and Jones, 1988; Astiz and Shearer, 2000). Cross-sections of earthquake hypocenters (3D locations) in Figure 2-5 show the complex vertical distribution of the earthquakes (Legg, 2021).

Relocation of the hypocenters (Latitude, Longitude, Depth coordinates) for events recorded since 1981 used advanced waveform cross-correlation techniques (Hauksson *et al.*, 2012) and 3D seismic velocity models (Hauksson, 2000) to provide more accurate images of earthquake distributions in the southern California crust (Figures 2-4 and 2-5). The solid dots show the most accurate relocations and red symbols have the best depth estimates. These 3D earthquake locations show that both vertical (predominately strike-slip) and moderate-to-low angle faults (possible blind thrusts) are seismically-active offshore southern California. It also appears that some earthquakes occur very deep in the crust and possibly within the upper mantle (below MOHO[3]).

This report reviews the advancements in understanding the active faulting that determines the earthquake potential affecting the SONGS site. Changes in seismic hazard estimates over the two decades since the 2001 study, are discussed, and new information is provided to compare with the previous investigations. In particular, recent large, complex, multi-fault, earthquake ruptures provide important evidence for the severity of earthquake hazards in California and elsewhere around the world. Deformation observed in excavations along the North San Diego County coastal zone is consistent with large prehistoric earthquakes in the San Onofre region

[3] Mohorovičić discontinuity (MOHO) is the boundary between the crust and the mantle in the earth.

(Kuhn, 2005). The Southern California Earthquake Center (SCEC) has led much of the research for such events in California and works closely with SCE and consultants responsible for evaluating these hazards and designing damage mitigation strategies.

The updated UCERF3 was published after the GeoPentech (2010) report, and SCEC, working with the USGS and National Science Foundation, continue to update the Community Fault Model (CFM) used for comprehensive assessment of earthquake hazards in California. Another update of the SCEC CFM and USGS Quaternary Fault Model used for the National Seismic Hazard Mapping Program is also planned (S. Marshall, 2022, Personal Communication).

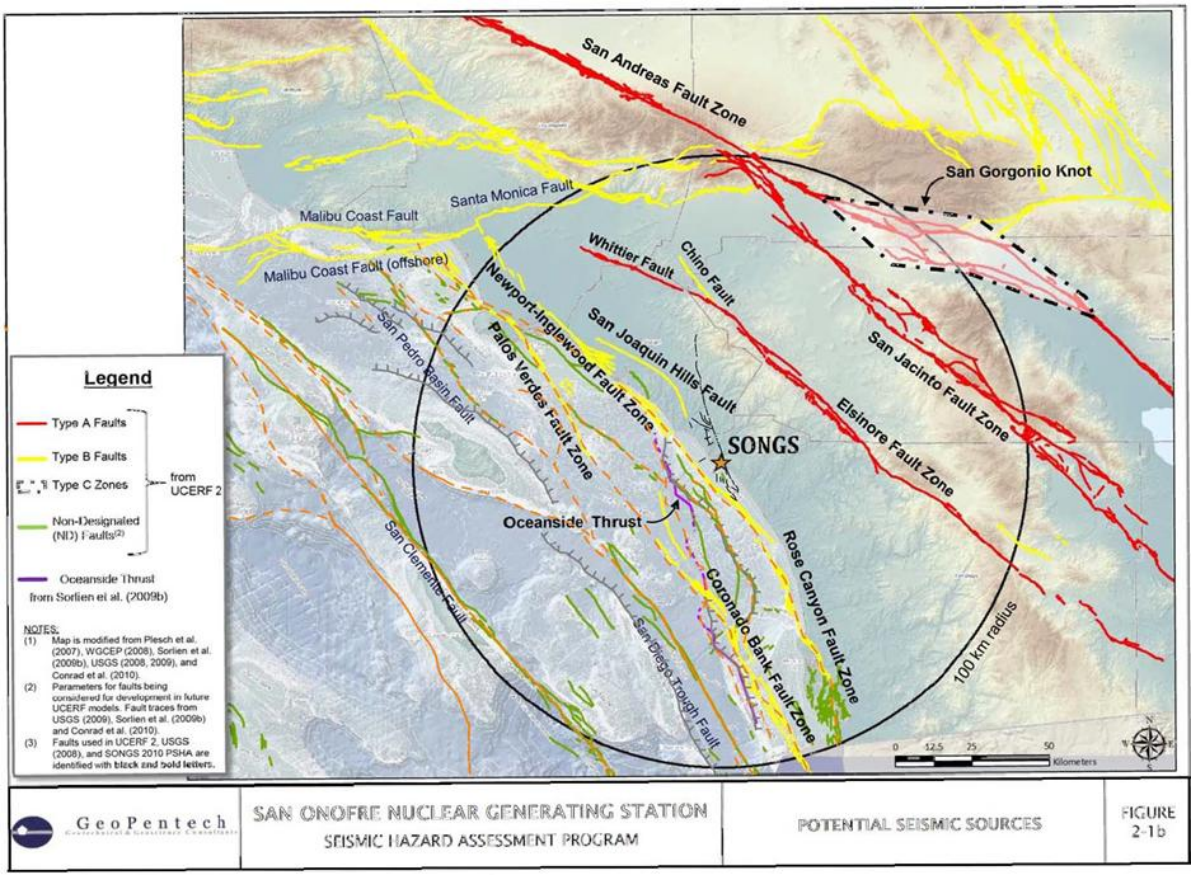


Figure 2-2. Potential seismic source map (GeoPentech, 2010) with updated UCERF3 faults in orange, and upper tips of detachments (Sorlien *et al.*, 2015), black with hashes in dip direction.

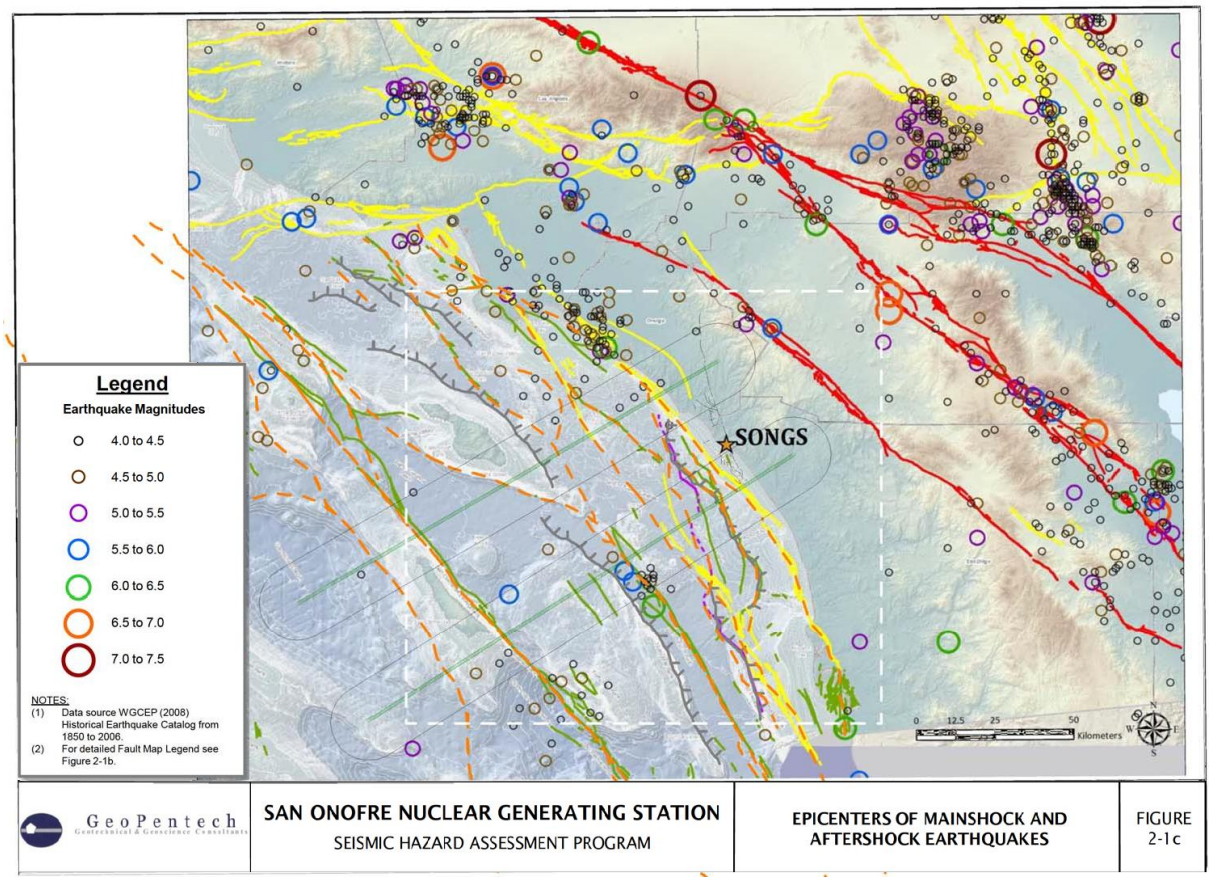


Figure 2-3. Southwest California historic earthquakes, 1850-2008 (GeoPentech, 2010) are Seismicity cross-sections (green lines) with 15-mile wide buffers (Legg, 2020).

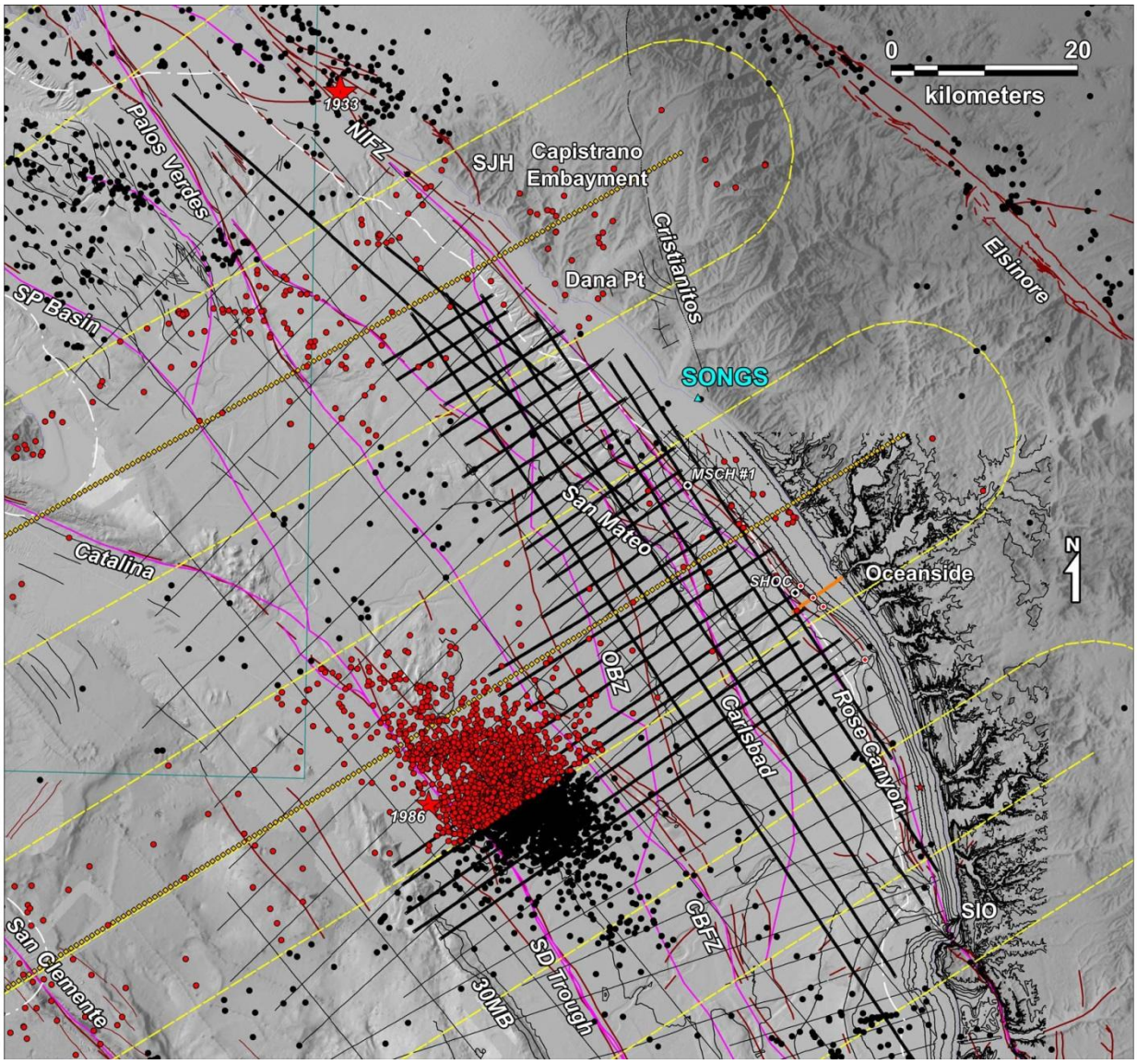


Figure 2-4. SONGS with 1981-2019 magnitude M>2 relocated earthquake positions. Earthquake data from Hauksson *et al.* (2012), red dots in cross-sections.

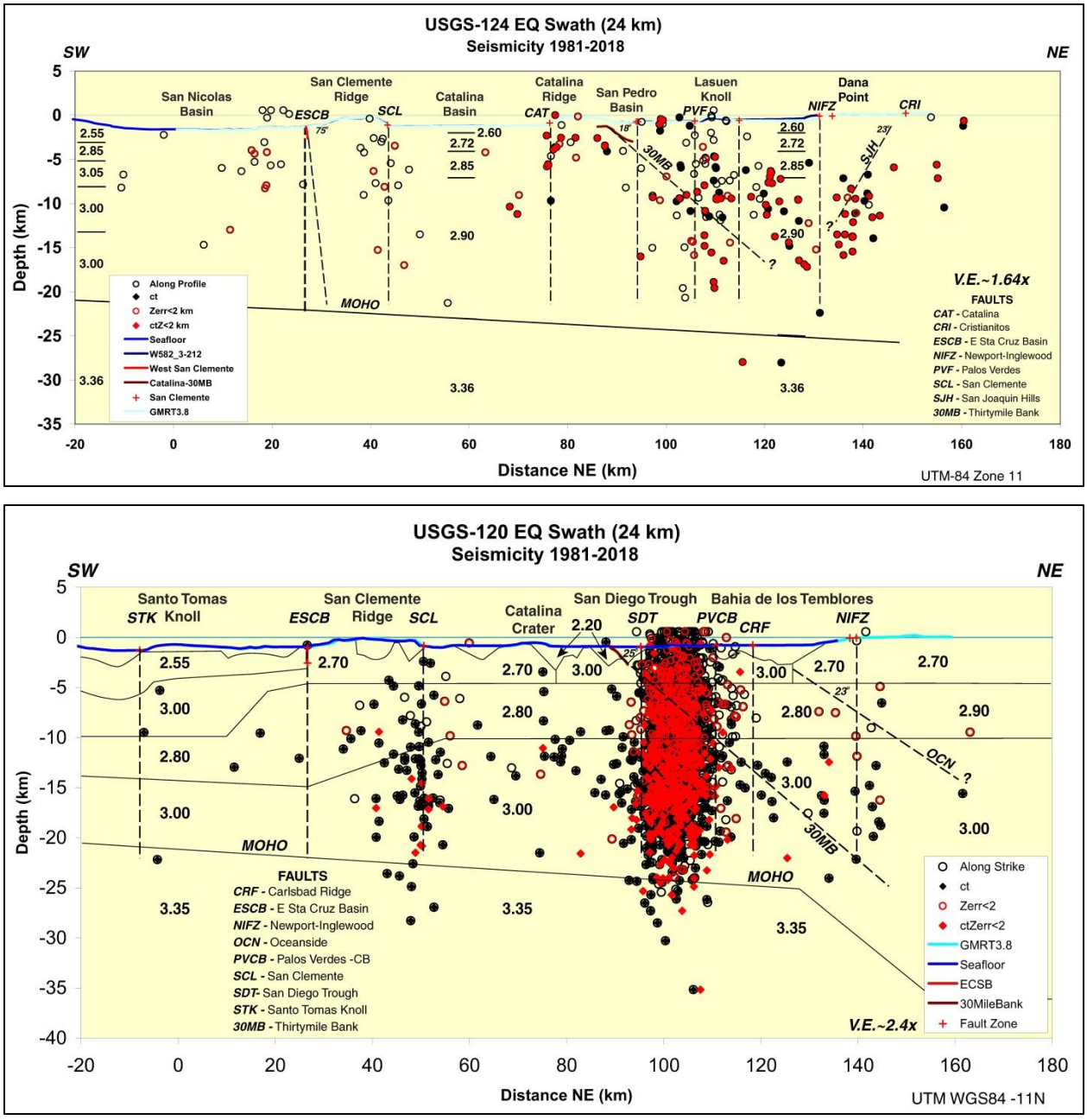


Figure 2-5. Earthquake swath profiles across the Inner Borderland offshore San Onofre. Data from Hauksson *et al.* (2012), upper, and 2019 update, lower.

2.2 GROUND SHAKING HAZARDS

Fault rupture and slip in the brittle upper crust produce seismic waves that propagate through the earth and along the surface to great distances from the source fault(s). Strong ground shaking may damage buildings and other structures and produce ground failure, including surface fault rupture with offset of the ground and structures across the active fault zone. Secondary ground failures including liquefaction of susceptible materials below the ground surface or failure of slopes may be induced in areas of strong shaking. For seismic hazard assessment, identification of faults in the region that may produce potentially damaging earthquakes (*seismogenic* faults) must be identified, mapped, and characterized for estimation of earthquake effects (Figure 2-2).

Ground shaking hazard is dependent upon the *magnitude* of the earthquake; *distance* of the site from the fault rupture; *direction* of propagation for the fault rupture (*directivity*); and, for the seismic waves, *geologic conditions* along the seismic wave path, *local soil conditions* for wave amplification, and possible *resonant basin effects* (Kramer, 1996). Mathematical formulations called *attenuation relationships or ground motion prediction equations (*GMPE*)*, based on empirical data from historic earthquakes, are used to estimate the expected shaking levels for earthquake scenarios using the modeled fault surfaces, measured distance from the fault to the site, and amplification factors for the site-specific soil conditions.

Seismic waves propagate at a wide range of frequencies, from short-period compressional waves (*P-waves*) to moderate and long-period shear waves (*S-waves*), which propagate through the crust (*body waves*). Long period surface waves propagate along the earth surface and attenuate at slower rates than body waves. Shear waves and surface waves produce strong horizontal accelerations that cause damage to structures built to withstand mainly vertical gravity forces but may lack strength to withstand these horizontal forces.

Buildings and other structures respond differently to earthquakes according to the natural resonant frequency of the structure and the type of waves. P-waves travel fastest and arrive first, followed by shear waves and long-period surface waves, which tend to produce greater shaking amplitudes. Attenuation relationships account for all types of waves but are based upon the maximum amplitudes recorded during earthquakes at each observation site. Digital recordings of the seismic waves from earthquakes are processed to create response spectra – charts of amplitude versus wave frequency, which can provide important information for structural engineering design and damage assessment. The Probabilistic Seismic Hazard Assessment (PSHA) considers several response spectral periods (inverse of frequency) that are relevant to the structures of concern. For critical structures, a fully dynamic earthquake rupture and seismic wave propagation model can be used to produce realistic earthquake strong-motion time-histories (*seismograms*) to evaluate structural response to earthquakes.

2.2.1 Seismogenic Faults

Numerous faults have been mapped in the SONGS coastal and offshore region that are aligned with the northwest trend of the coast and the Pacific-North America transform plate boundary (Clarke *et al.*, 1987; Fischer and Mills, 1991; Plesch *et al.*, 2007; Maloney *et al.*, 2016; Sorlien *et al.*, 2016; Sahakian *et al.*, 2017; Conrad *et al.*, 2019). The most prominent coastal fault

zone is the NIRC mapped from Santa Monica to San Diego Bay and continues south along the northern Baja California coast as far as the Agua Blanca fault at Punta Banda, offshore Ensenada (Legg, 1985; Legg *et al.*, 1991; Ryan *et al.*, 2009). The Palos Verdes, Coronado Bank (CBFZ), San Diego Trough and San Clemente fault zones are other prominent faults within 60 miles offshore from San Onofre. Few Quaternary faults are located onshore in the coastal region between Dana Point and Oceanside. The prominent N18°W-trending Cristianitos fault crosses the shoreline about one mile southeast of San Onofre (Ehlig, 1979; Shlemon, 1987). The Elsinore fault is located about 25 miles east of San Onofre and represents one of the more significant active faults in southern California (Kennedy, 1977; Jennings, 1994). It was considered in the seismic hazard assessments for construction of the power plant (GeoPentech, 2010) and ISFSI.

Immediately offshore of SONGS is the South Coast Offshore section of the Newport-Inglewood fault zone, which links with the Rose Canyon fault zone forming a major *Coastal Fault System* (Legg, 1985; Legg, 1991; Grant and Rockwell, 2002; Legg *et al.*, 2018) that reaches from the Los Angeles Basin to Bahía Todos Santos in northern Baja California. A *fault system* is a collection of faults and fault zones that interact to accommodate tectonic plate motion. For example, the San Andreas Fault System comprises all of the major faults and fault zones along the Pacific-North America transform plate boundary in California (Wallace, 1990). The San Mateo, Carlsbad, and San Onofre fault zones (Conrad *et al.*, 2019) appear connected with the NIRC in the Coastal Fault System forming a complex zone of tectonic deformation that includes horizontal strike-slip and oblique reverse-slip on non-vertical faults. Seismic reflection profiles provide the major data used to map this submerged fault zone, but few deep penetration exploration industry profiles (Figure 2-4, reprocessed data, thick black lines) exist within the California State Lands boundary (Maloney *et al.*, 2016). Consequently, the deep structure of this fault zone is poorly known near the coast just offshore of the ISFSI.

Accurately located hypocenters of seismicity shown in Figures 2-4 and 2-5 recorded by the Southern California Seismograph Network (SCSN), show the complicated spatial distribution of seismicity associated with the complex array of shallow fault traces mapped in the area. Major clusters of seismicity span 3-6 mile wide swaths between mapped faults as seen in the area of the 1986 M_S5.8 Offshore Oceanside earthquake sequence (Hauksson and Jones, 1988; Astiz and Shearer, 2001; Legg *et al.*, 2015). A somewhat narrower northwest alignment of epicenters exists along the Newport-Inglewood fault zone where the 1933 M_S6.2 Long Beach earthquake initiated (Hauksson and Gross, 1991).

2.2.2 Probabilistic Seismic Hazard Assessment

A Seismic Hazard Assessment (SHA) considers all earthquake sources within about a 60-mile radius that may produce surface fault rupture, strong shaking, secondary ground failures including liquefaction and slope failure, and tsunami generation in coastal areas. Two analysis techniques are used in an SHA: (1) deterministic analysis, which models specific earthquake scenarios to estimate the maximum effects of large earthquakes at a site, and (2) a Probabilistic Seismic Hazard Assessment (PSHA), which is used to account for uncertainty in the levels of hazard that may be produced from many different potential earthquakes on numerous faults with different frequencies of earthquake production. In complex areas of tectonic deformation, along broad tectonic plate boundaries as exist in southern California, fault zones or systems with

multiple fault segments and zones must be considered carefully. GeoPentech (2010) produced a thorough SHA at the SONGS facility based on the Unified California Earthquake Rupture Forecast, Version 2 (UCERF2, WGCEP, 2008). This analysis was "state-of-the-art" and used fault and recurrence models available at that time.

Subsequent investigations provided new or updated data based on reprocessing and interpretation of existing exploration industry Multichannel Seismic Reflection Profiling (MCS) data, acquisition of new high-resolution, moderate-to-shallow penetration (upper kilometer) MCS data, and digital single-channel seismic data (Sorlien *et al.*, 2015; Maloney *et al.*, 2016; Sahakian *et al.*, 2017; Conrad *et al.*, 2019; Holmes *et al.*, 2021). Completion of the third version of the Unified California Earthquake Prediction Model (UCERF3, 2013) included three deformation models to reduce uncertainties in the time-independent source model. The three models were based on kinematically-consistent inversions of geodetic and geologic data, which helped provide some constraints on slip rates for faults lacking geologic data.

Alternate models, including multi-fault ruptures, were considered in the inversion. Continuous acquisition of digital seismograms for southern California regional earthquakes expanded the historical event database with more accurate locations and magnitudes. Relocation of the hypocenters (Latitude, Longitude, Depth coordinates) for events recorded since 1981 used advanced waveform cross-correlation techniques (Hauksson *et al.*, 2012) and 3D seismic velocity models (Hauksson, 2000) to provide more accurate images of earthquake distributions in the southern California crust (Figures 2-4 and 2-5). Interpretations made in 2010 require reviews and updates to incorporate the greater knowledge obtained in the past decade necessary for more accurate evaluation of the seismic hazard at the site.

The *Strike-slip Seismic Source Characterization Model* for the NIRC fault zone (section 2.1, GeoPentech, 2010) is based on the wrench tectonics mode of deformation (Wilcox *et al.*, 1973; Sylvester, 1984; 1988). As stated by GeoPentech: *"This theory is compatible with the presence of shorter, shallower dipping, normal and thrust subsidiary faults in a system dominated by high--angle, through-going primary strike-slip fault."* The wrench tectonics model has been used successfully to predict or interpret structure at depth for petroleum exploration. However, proper application of the theory requires careful consideration of boundary and initial conditions in the model. Existing geologic structure resulting from a prolonged (20-100+ million years) tectonic evolution of the Pacific and North America plate boundaries that involved subduction and oblique -rifting before creating the current transform plate boundary dominated by the onshore San Andreas strike-slip fault.

Active faults within the San Andreas fault system include the full range of tectonic deformation styles-low-angle thrusts (blind or surface breaching), moderate to low-angle normal faults (Basin-and-Range, Continental Borderland), and both parallel and oblique strike-slip faults (San Andreas, San Jacinto, Elsinore, San Clemente, San Diego Trough, Newport-Inglewood). Initially considered the South Coast Offshore fault zone (Barrows, 1974; Ehlig, 1977), 50 years of investigation led to recognition of the Coastal Fault System as a combination of high-angle strike--slip, oblique-reverse, and low-angle detachment faults (Clarke *et al.*, 1987; Fischer and Mills, 1991; Rivero *et al.*, 2000; Ryan *et al.*, 2009; Rivero and Shaw, 2011; Sorlien *et al.*, 2016; Maloney *et al.*, 2016; Sahakian *et al.*, 2017; Conrad *et al.*, 2019).

Seismicity demonstrates the activity of numerous faults within this complex zone of deformation (Figures 2-3 and 2-4, Legg, 1980; Legg, 1987; Nicholson and Crouch, 1989; Legg and Kennedy, 1991; Grant and Shearer, 2004; Legg, 2021). Fault interaction within this fault system may produce large, complex, multi-fault, multi-segment, earthquakes (Legg *et al.*, 2018). Both horizontal strike-slip and vertical dip-slip components result to accommodate the northwest translation of the Pacific Plate with its Borderland and Baja California captured microplates (Figure 2-1) along the continental margin.

2.2.3 Methods of the GeoPentech 2010 PSHA

Ground shaking hazard is dependent upon the magnitude of the earthquake, distance of the site from the fault rupture, direction of propagation for rupture and seismic waves, geologic conditions along the seismic wave path (ray path), local soil conditions for wave amplification, and possible resonant basin effects (Kramer, 1996). Mathematical equations called *attenuation relationships*, based on empirical data from historic earthquakes, are used to estimate the expected shaking levels for earthquake scenarios using the modeled fault surfaces, distance from the fault to the site, and amplification factors for the site-specific soil conditions. A new generation of Ground Motion Prediction Equations (GMPE), (Abrahamson and Silva, 2008; Boore and Atkinson, 2008) were used for the 2010 investigation. Development of improved GMPE has continued based on additional data from recent California and global earthquakes.

Seismic waves propagate at a wide range of frequencies, from short-period compressional waves (P-waves) to moderate and long-period shear waves (S-waves) and surface waves. Buildings and other structures respond differently to earthquakes according to the natural resonant frequency of the structure and the type of waves. P-waves travel fastest and arrive first, followed by shear waves and long-period surface waves, which tend to produce greater shaking amplitudes. Attenuation relationships account for all types of waves but are based upon the maximum amplitudes recorded during earthquakes at each observation site.

Digital recordings of the seismic waves from earthquakes are processed to create response spectra – charts of amplitude versus wave frequency, which can provide important information for structural engineering design and damage assessment. The PSHA considers several response spectral periods (inverse of frequency), which are relevant to the structures of concern. For a rigid structure like the ISFSI, peak ground acceleration (PGA) is an appropriate measure for the earthquake forces. Horizontal ground motions are typically considered as most buildings can withstand vertical forces (gravity) but must be constructed to resist the strong lateral motions produced by earthquakes.

GeoPentech (2010) defined two "end member" fault model cases for estimating the seismic hazard at SONGS. The "strike-slip" end member consisted of the various segments of the NIRC fault zone; the second "blind thrust" end member consisted of the various models for the OBT and related faults – "wedge/thrust" model of Rivero *et al.* (2000); Rivero, (2004), and Rivero and Shaw (2011). Based on lack of evidence confirming the Pleistocene or younger activity on the OBT as a major through-going thrust fault, GeoPentech (2010) applied relatively low weight in the PSHA for this end member source model. Interaction between the OBT and strike-slip faults was not directly modeled, reasoning that the PSHA with the two models would average out these effects and provide an assessment of the seismic hazard potential (*risk*).

2.2.4 Seismic Sources

Past evaluations of the seismic hazard at sites throughout California including SONGS have relied on the Alquist-Priolo Act (AP) definition of active faults based on evidence for Holocene, less than 11,700 year-old fault rupture (surface faulting). The AP definition applies to surface fault rupture hazards. Fault rupture that produces tectonic earthquakes initiates deep, (typically 3-12 miles; Figure 2-5) within the Earth's brittle crust. Therefore, recent large earthquake that occurred on faults were unknown or not recognized as active.

Most earthquake ruptures fail to reach the ground surface. Moderate to large earthquakes (M>5) on "blind" faults cause substantial damage without producing surface rupture, as for example, did the 17 October 1989 M_w6.9 Loma Prieta (Plafker and Galloway, 1989), and 17 January 1994 M_w6.6 Northridge (Teng and Aki, 1996) earthquakes. Furthermore, there have been several large (M7+) earthquakes striking southern California in the past few decades on faults that were either unmapped, or unrecognized as active ("Holocene"), or capable of producing large earthquakes. In particular, the 28 June 1992 M_W7.5 Landers (SCEC, 1992), 10 October 1999 M_W7.1 Hector Mine (Rymer *et al.*, 2002), 4 April 2010 M_W7.5 El Mayor-Cucapah system (Fletcher *et al.*, 2014), and July 2019 M_W6.6 and M_W7.4 Ridgecrest (SCSN, 2019) earthquakes provided abundant data to educate the earthquake science community about large, complex, multi-fault earthquake ruptures on previously unidentified or poorly known faults. The faults located offshore SONGS fit in that category where better models of such fault interactions are needed to provide more accurate earthquake hazard assessments.

Earthquake history and recent seismicity data from SCSN and other seismograph networks in California and beyond provide important data to identify active faulting below ground and offshore. Advances in digital technology and computer algorithms to locate earthquake hypocenters, the latitude, longitude, and depth, more accurately are now able to delineate many buried or offshore fault zones (Figure 2-5; Hauksson *et al.*, 2012). Every significant earthquake in California and elsewhere brought new understanding and revision of seismic hazard estimates. Furthermore, improvements in data acquisition and processing for mapping offshore geologic structure and stratigraphy include multichannel seismic profiling systems, other geophysical methods, and Global Positioning System (GPS) for navigation.

Seismic stratigraphy as a method for more accurate sub-seafloor mapping and stratigraphic interpretation of geologic history provide better estimates of timing prehistoric activity and slip rates on faults. However, the weak link remains the lack of deep penetration boreholes or wells offshore to constrain the age of the seafloor stratigraphic sequences. Fortunately, there are two exploration wells located offshore near San Onofre (MSCH#1 and SHOC, Figure 2-4). Sorlien *et al.* (2016) traced prominent seismic reflection horizons from the abundant seismic profiles and well data from San Pedro Bay to San Diego to provide a coarse stratigraphic correlation for timing deformation and fault activity. The USGS (Normark *et al.*, 2009; Conrad *et al.*, 2019) used shallow piston cores in the area to determine the Holocene and Quaternary horizons in high-resolution seismic profiles. Stratigraphic thickness maps offshore southern California (Sorlien *et al.*, 2016) show late Quaternary uplift (post-600 ka) along the San Mateo-Carlsbad fault zone (Figure 2-6).

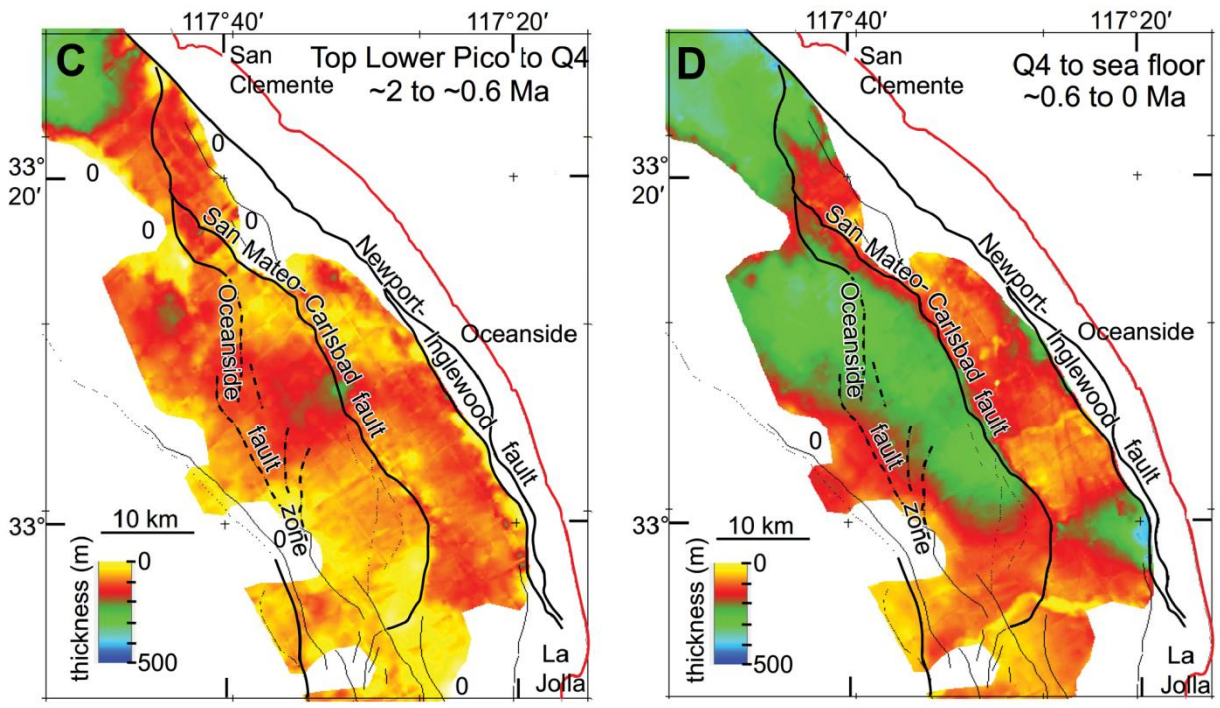


Figure 2-6. Thickness of late Quaternary sediments in the Inner Borderland between Dana Point and La Jolla (Sorlien *et al.*, 2016). Thick sediments (green) west of San Mateo-Carlsbad fault show uplift occurred during late Quaternary.

2.2.5 Seismic Risk

SCE has worked with the SCEC and other earth scientists to update the seismic hazard model for SONGS (GeoPentech, 2010). Research accomplished in the past decade since the 2010 GeoPentech report includes substantial interaction with SCEC scientists at meetings and workshops held to review ongoing research regarding the regional geology and earthquake hazards. In 2011, a workshop was held for the update of the Unified California Earthquake Risk Forecast (UCERF), which has been updated to version 3 (UCERF3, 2013). The main improvement in the model is to include the potential for multi-fault ruptures that produce large (M>7) earthquakes. This change reduces the probability (frequency) of moderate earthquakes (M5-7), which is more consistent with the historical record of California seismicity. The previous model suggested more frequent moderate magnitude events than have been observed in the historic record since about 1875.

The multi-fault rupture concept was adopted in the 2010 GeoPentech report by considering alternative fault configurations and rupture scenarios for the primary faults that affect the SONGS location. In particular, different configurations of the NIRC fault zone, as well as deep slip on the OBT, were considered in the PSHA. The models used were restricted to the vertical strike-slip faulting of the NIRC separately from the low-angle thrust faulting of the OBT. The NIRC-OBT combination dominated the PGA hazard for longer return periods (>600-700 years). The Elsinore, San Jacinto and San Andreas Class A faults (well-defined with slip rates>5 mm/yr) dominate the short return period hazard.

According to the California Coastal Commission staff report for the SONGS Holtec ISFSI CDP (CCC, 2015), strong-motion hazard for the 10% chance of exceedance during a 50-year interval risk level, 475-year return period that is used for building codes, the expected horizontal PGA is 0.227g, or about one-quarter gravitational acceleration. For the 100-year return period, the expected PGA drops to 0.11g. The Design Basis Earthquake (DBE) for a M7.0 event at 5 miles from SONGS was computed to be 0.31g. The design value with safety factor was set at 0.67g, which has an estimated return interval of ~7,100 years[4]. The SONGS ISFSIs are designed to withstand 1.5g in each horizontal direction (2.12g vector sum), and 1.0g vertical.

The Annual Frequency of Exceedance risk of strong ground motion levels was reduced in the 2010 PSHA compared to the 1995 PSHA (Figure 2-7). Increasing the maximum magnitudes by including multi-fault ruptures reduces the frequency of moderate earthquakes (M5-7), which define the short term hazard. Note that shaking level (weighted spectral acceleration) for the longest return period of 10,000 years, was only slightly reduced. This return period is important for the nuclear hazard issues, but for the short period of concern to the California Coastal Commission requirements (15-30 years or until 2050), expected shaking levels were reduced to about 0.2g (from 0.3g or 33% decrease at the 100-year return period). The NIRC was assigned a weight of 88% compared to the 12% used for the OBT and represented the significant earthquake source.

[4] The California Geological Survey (CGS) and U.S. Geological Survey (USGS) have carried out independent evaluations of earthquake ground shaking hazards. The CGS Earthquake Shaking Potential Map for California portrays the San Onofre areas as region of relatively low ground shaking potential (Branum et al., 2008). With a PGA of 0.67 the recurrence interval is 7,143 years (GeoPentch, 2010).

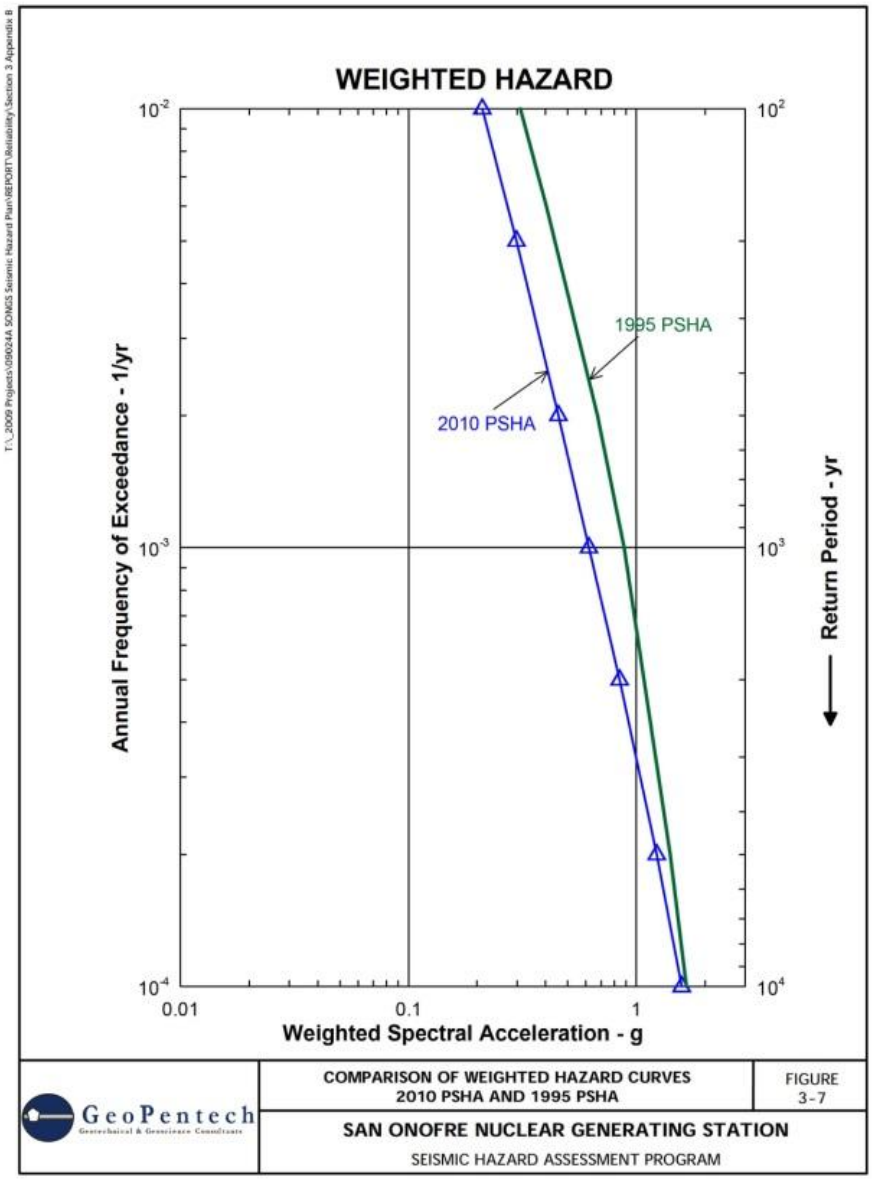


Figure 2-7. Comparison of hazard curves 2010 PSHA and 1995 PSHA. From GeoPentech (2010, Figure 3-7).

2.2.6 Coastal Fault System

The recent investigations of the Coastal Fault System supported by SCE (Maloney et al. 2016; Sahakian et al, 2017, Holmes et al, 2021) and the USGS (Conrad et al. 2019) provided a more accurate mapping of the shallow crustal faulting beyond the California State Lands boundary. The reprocessed deep-penetration exploration industry MCS survey data (Maloney et al. 2016) were used to evaluate a broad blind thrust fault model (Rivero and Shaw, 2011; Rivero et al., 2000) and compare with strike-slip or wrench fault models for tectonic deformation along the Coastal Fault System. The strike-slip model for the Newport-Inglewood-Rose Canyon fault zone was used for previous earthquake hazard evaluations at SONGS (GeoPentech, 2010). The deep seismic imaging of the fault zones showed the significance of fault bends and stepovers that produce significant vertical deformation in addition to the dominant strike-slip. Better imaging and understanding of the faulting on the continental slope was obtained and was sufficient to demonstrate zones of oblique faulting with components of reverse-slip at restraining fault geometries (left bends or stepovers) and normal slip at releasing fault geometries (right bends or stepovers). The characteristic downward convergent fault geometry known as "flower structure" (Wilcox et al. 1973) was recognized.

Sorlien et al (2016) mapped the Inner Continental Borderland from San Pedro Bay to San Diego using exploration industry MCS profiles available through the USGS National Archive of Marine Seismic Surveys (NAMSS) and recognized several major fault bends and stepovers with oblique-slip including those offshore La Jolla, Carlsbad, and San Onofre. An important observation of these studies is the recognition of the change from an extensional (transtension) to a convergent (transpressional) faulting style that occurred near the Miocene-Pliocene time period (about 6 Million years ago). This change in tectonic style, related to changes in the Pacific-North America plate boundary relative motion (Lonsdale, 1991) correlates with the eastward jump of the plate boundary to form the Gulf of California system of strike-slip transform faults and extensional spreading centers.

The result of this fundamental change in the plate boundary system caused former releasing bends and pull-apart basins within the Inner Continental Borderland (and Los Angeles Basin) to become transpressional "pop-up" structures, inverting the former structural basins (Legg et al. 2007). Maloney et al. (2016) concluded that activity on the OBT modeled by Rivero and Shaw (2011) ceased in Pliocene time and suggested the strike-slip model for the NIRC fault zone was appropriate for evaluating large earthquake potential at San Onofre. Sahakian et al. (2017) provided updated mapping and evaluated the potential for large, complex, multi-segment fault ruptures involving the NIRC including oblique-slip at bends and stepovers. Use of Coulomb failure criteria to infer probability of rupture propagation jumping to adjacent segments provided models for estimating maximum magnitudes and likelihood of occurrence. What appears to have been overlooked by these strike-slip models and the blind fault models is the fact that a system of major low-angle detachments, i.e., the Thirtymile Bank and Coronado Bank – Oceanside faults (Sorlien et al. 2016) underlie these steep-dipping faults of the Coastal Fault System.

The San Onofre coast is located at the hinge between uplift and subsidence induced by large-scale transpression across this region south of the San Andreas Bend Region. The Coastal Fault System, comprised of the NIRC strike-slip fault zone along the continental shelf and the San Mateo-Carlsbad oblique-reverse faults located along the base of the continental slope, may

present a severe earthquake hazard. The existence of the OBT and deeper Thirtymile Bank detachment as low-angle slip surfaces may facilitate linkage between the high-angle strike-slip faults to produce large, complex, multi-fault earthquake ruptures (Legg *et al.*, 2018). For example, the 2019 M_W7.8 Kaikōura, New Zealand earthquake (Hamling *et al.*, 2017) produced substantial surface rupture on at least 12 shallow faults underlain by a major blind thrust fault associated with oblique subduction beneath the north end of the South Island. In addition to the severe ground shaking and deformation, a tsunami (up to 3m at Kaikōura) was observed along the coasts adjacent to the vertical fault displacements.

Deformation recognized and mapped in the coastal zone near SONGS (Carlsbad; Kuhn, 2005), appears consistent with large prehistoric coastal earthquakes. Observed deformation and related features include paleo-liquefaction sand blows, injection dikes, and lateral spread surfaces, severe and widespread ground fracturing, secondary faulting, and tsunami deposits (Figures 2-8 and 2-9). The liquefaction involved Pleistocene, and dense Eocene sands, which were injected through overlying late Quaternary soils and Holocene Indigenous habitation sites. Liquefaction of dense sands requires extreme shaking from a large, nearby fault source. The complexity of faulting along the Coastal Fault System (NIRC and related faults) combined with the existence of at least two (Oceanside and Thirtymile Bank) detachment/blind thrust/oblique-reverse surfaces beneath the entire coastal zone from (at least) Huntington Beach to San Diego represents the prime suspect for producing such large coastal earthquakes. Historic seismicity confirms fault activity in the area.

In addition to surficial deformation, coastal uplift including the San Joaquin Hills and late Pleistocene marine terraces document late Quaternary and possibly Holocene activity (Grant *et al.*, 2002). Recent work on coastal marine terrace uplift shows that subsidence may also occur (Castillo *et al.*, 2019). Offshore research with seismic reflection imaging recognized progressive tilting of Pleistocene and older surfaces that suggest overall subsidence of the Inner Borderland (Sorlien *et al.*, 2009; Sorlien *et al.*, 2016). Progressive tilting at the hinge of a mega-fold (syncline) along the coast may explain the apparent lack of Holocene marine terrace near SONGS (Rockwell, 2018 personal communication).

Based on the repetitive lateral spread surfaces[5] within marine terrace deposits located above the wave-cut platform Marine Isotope Stage 5e (MIS-5e, 125 ka), the recurrence interval for such large earthquakes is about 10,000 years.

[5] Liquefied sand layer that enables more competent material above to slide laterally down gentle slopes.

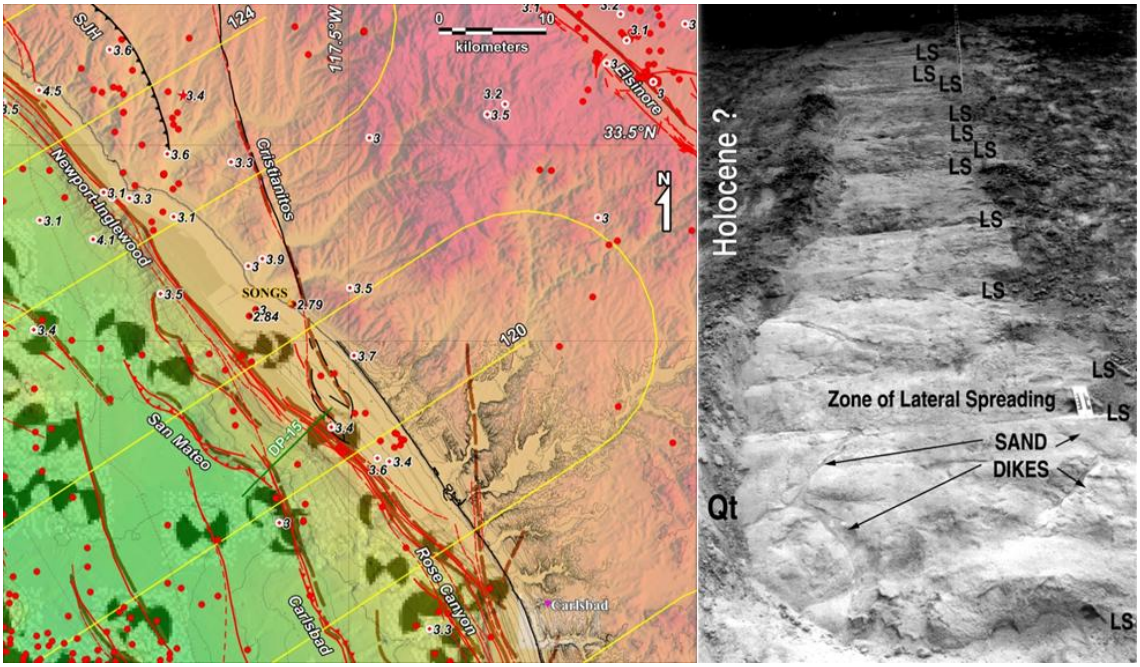


Figure 2-8. Map (left) and photograph (right) of paleoliquefaction sites exposed in a cut slope along Encinas Creek, Carlsbad. Repeated lateral spreads (LS) record at least 12 large prehistoric earthquakes. (Kuhn, 2005).

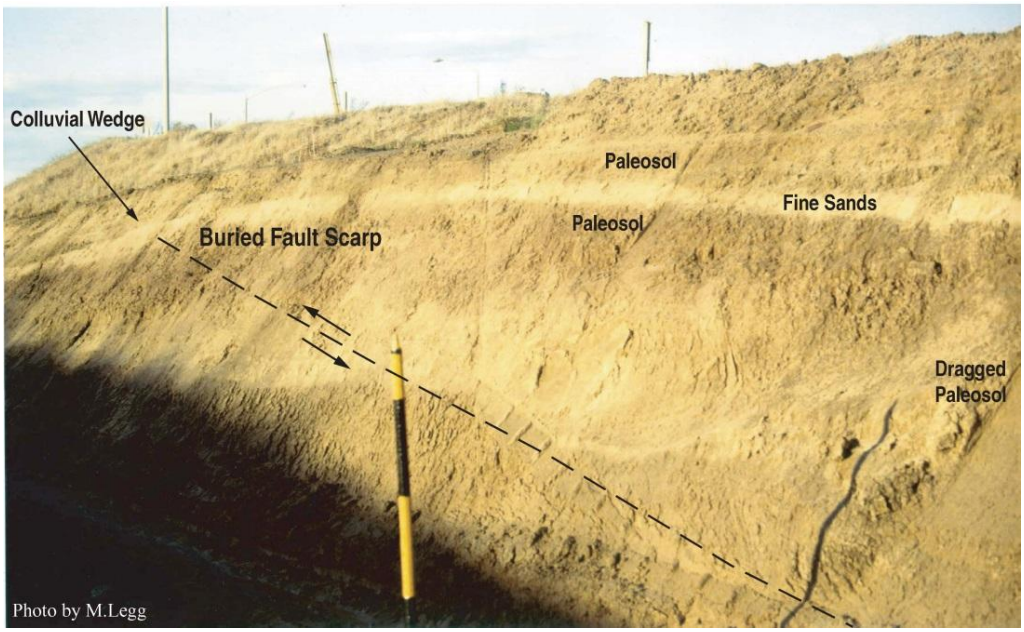


Figure 2-9. Photograph of paleo-earthquake fault rupture with liquefaction sand deposits covering 40,000-yr soil and fault scarp (Kuhn, 2005; Legg *et al.*, 2018). Fault continues above paleosol an unknown distance into vegetated slope area.

2.2.7 Hypothetical M_W7.6 Scenario Earthquake

In this section, we provide estimates for seismic hazards anticipated (and observed) from extreme (M_W>7) events to compare with the design criteria provided for the ISFSI and SONGS facilities. The complex pattern of faulting observed following the 14 November 2016, M_W7.8 Kaikōura earthquake in New Zealand (Hamling *et al.*, 2017), resembles updated mapping of the Coastal Fault System described in previous sections. Shaking with PGA exceeding 1.0g horizontal and vertical directions was recorded in Kaikōura (Jibson *et al.*, 2018). A similar event may strike the southern California coast (Legg *et al.*, 2018) reaching from Los Angeles to San Diego (Figure 2-10).

Here we describe a similar model for a M_W7.6 Coastal Fault System event that extends from Huntington Beach to La Jolla, excluding the strike-slip segments of the Newport-Inglewood fault zone, which ruptured in 1933, and the San Diego segments of the Rose Canyon fault, which ruptured in 1862 (Legg and Agnew, 1979; Singleton *et al.*, 2019). Nine fault segments defined include the South Coast section of the Newport-Inglewood fault zone (NIFZ), the Oceanside segment of the Rose Canyon fault zone, the San Mateo-Carlsbad fault zone, and the San Onofre Trend (SOT).

A continuation of the South Coast zone toward the southeast reaches the coast near the Agua Hedionda lagoon, which is bent to the southeast. Abundant paleo-liquefaction and surface fracturing from large prehistoric earthquakes have been mapped in that area (Kuhn, 2005). Details of the nine-segment fault rupture model, and two subset models (San Mateo-San Onofre-Carlsbad and NIRC fault sections) are described in the Local Tsunami hazards section. Subsidence at the north along the coast (blue shading) could be replaced by including reverse-slip on the San Joaquin Hills blind thrust (Grant *et al.*, 2002). Tsunami deposits found at Batiquitos Lagoon reached 22-30 ft above sea level (Kuhn, 2005).

Updated mapping of the NIRC fault zone (Sahakian *et al.*, 2017) recognized most of the fault segments originally defined by Fischer and Mills (1991) but missed nearshore faulting that lie inside the California State Lands three-mile limit. The new seismic profiles acquired by Scripps Institution of Oceanography were unable to cross into this area.

Exploration industry profiles available from the USGS NAMSS database (Treizenberg *et al.*, 2016) show a South Coast fault branch that trends toward the coast inside the continental shelf break offshore Oceanside (Figures 2-4 and 2-11). High-resolution seismic profiles show a tectonic dam produced by uplift along this fault segment (Figure 2-11). This creates a nearshore sedimentary basin where sediments from the coastal river deltas are channeled to the north to eventually empty into the deep basin along the San Mateo and San Onofre submarine canyons/slope gullies (Darigo and Osborne, 1986).

Multi-fault earthquake scenarios were evaluated by Sahakian *et al.*, (2017) using elastic dislocation modeling and Coulomb stress change to determine which stepovers between faults may fail when an adjacent fault slips. They concluded that the stepover near La Jolla was unfavorable for rupture continuation, but "*rupture along the full fault zone is possible*." The large M>7 earthquakes considered for the Coastal Fault System would be severe, but rare events with the long recurrence periods necessary to rebuild the tectonic strain (6-16 ft) at the slow 1-2

mm/yr slip rate. More frequent moderate earthquakes (M6-7) located close to the site define the seismic hazard response spectral values (GeoPentech, 2010).

The nine-segment earthquake source model representing the prominent offshore fault sections between Dana Point and La Jolla was used to evaluate the local tsunami potential at the SONGS ISFSI (CE, 2022-Section 7.5, Tsunami Hazards Analysis). The deformation model resembles that derived from the M_W7.8 Kaikoura earthquake with combined strike-slip and oblique reverse-slip on various segments. The largest local earthquake scenario consists of all nine segments with M_W7.62 (CE, 2022 in Table 7-5, source Local-sc1). Two other composite source models included the four segments of the Newport-Inglewood and Oceanside (Rose Canyon) strike-slip fault, with oblique-slip on the north and south segments of the South Coast Offshore fault (Table 7-5, source Local-sc3, M_W 7.41), and the San Mateo-San Onofre-Carlsbad oblique-reverse fault, with strike-slip on the San Onofre segment (Table 7-5, source Local-sc2 M_W 7.44).

Calculations of the expected PGA for the site were made for the nine-segment earthquake source model used in the Tsunami Hazards Analysis (Section 7.5). The closest horizontal distance of the site from the surface projection of the fault was measured as seven kilometers. Two different attenuation relations (ground motion prediction equations, GMPE) were used including the Joyner and Boore (1993; JB93) and Boore and Atkinson (2008; BA08) models. A site condition 'B' was used for the JB93 equation and a V_{S30} = 760 m/s equivalent to the B/C boundary site condition for the BA08 equation. Non-linear amplifications, which would take into account soft soils, were not considered because the SONGS site is based on a San Mateo bedrock formation that is the foundation of the site. The computed median PGA is 0.65g for the JB93 equation and 0.77g for the BA08 equation. These values are similar to the DBE with safety factor used for the power plant (0.67g). and well below the 1.50g used for the ISFSI design.

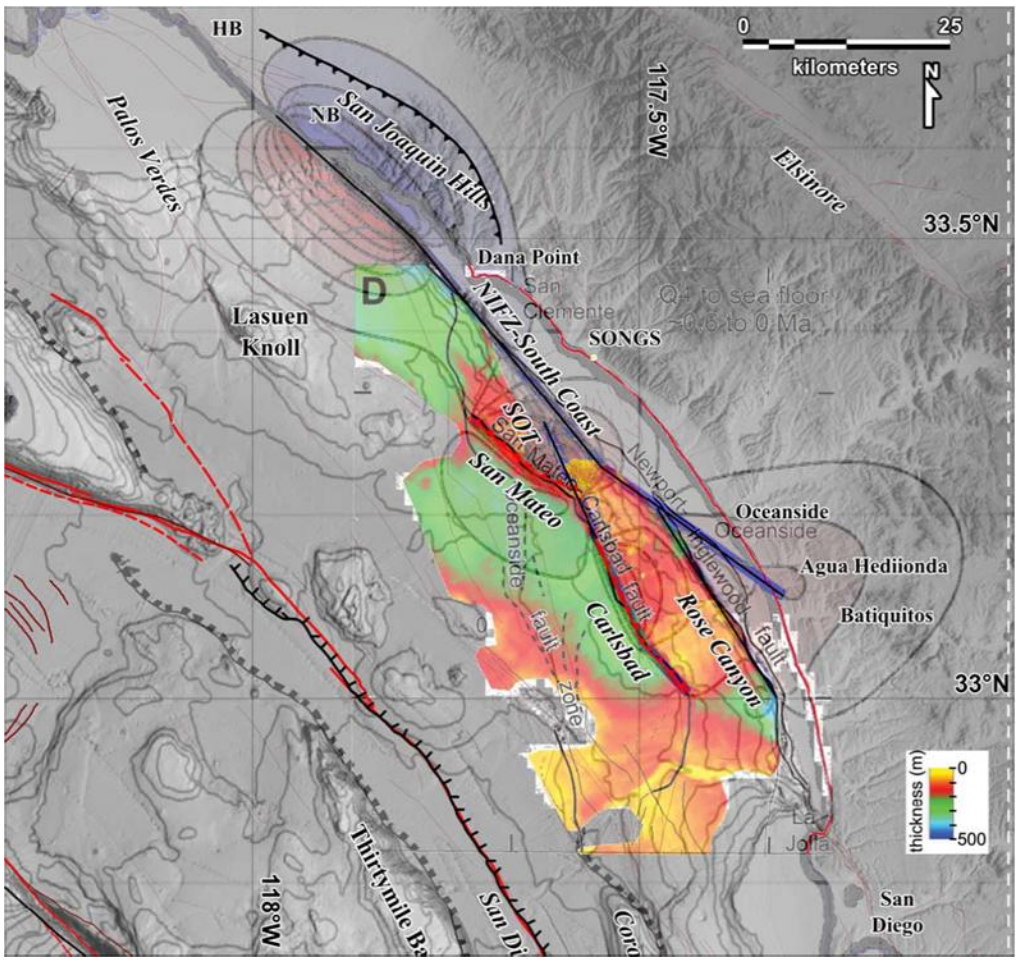


Figure 2-10. Map of simplified fault rupture model (thick lines with red-blue uplift contours) for MW7.6 earthquake along the Coastal Fault System. Sediment thickness overlay (Figure 2-6) of late Quaternary uplift along San Mateo-Carlsbad fault.

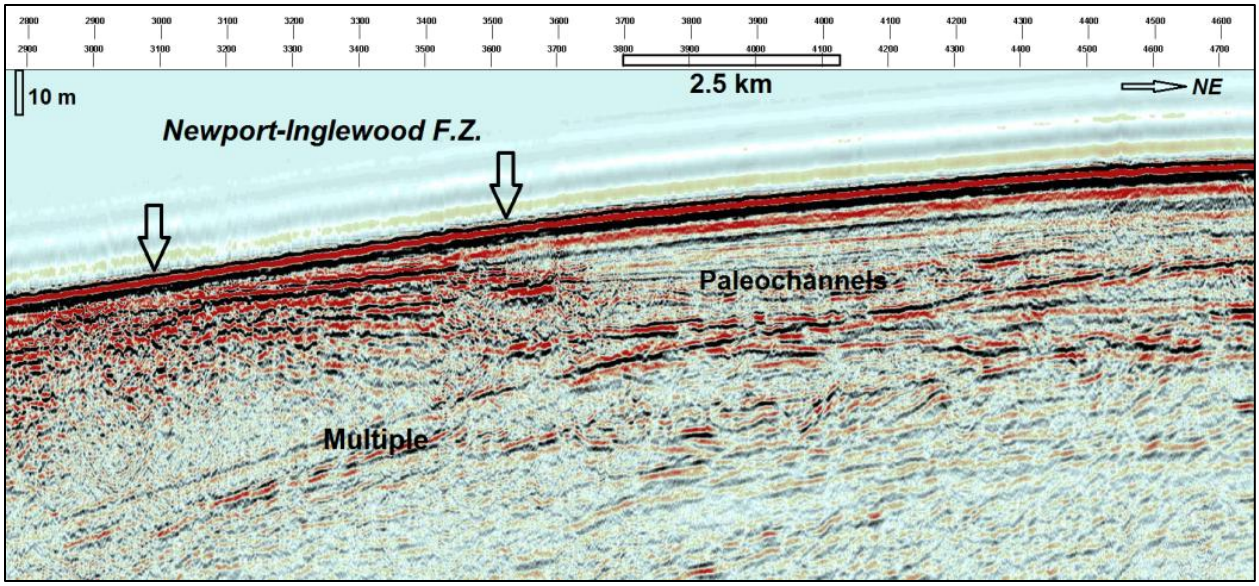


Figure 2-11. High-resolution 24-channel seismic profile of Newport-Inglewood fault uplift that blocks Quaternary paleochannels offshore Oceanside.

2.3 GROUND FAILURE HAZARDS

2.3.1 Surface Rupture

The Cristianitos fault is located about 0.75 miles west of SONGS (Figure 2-8). The fault is exposed in the coastal bluff to the south of SONGS where no evidence of rupture above the Eemian Interglacial 125 ka year old (OIS5e) marine terrace platform is observed (Shlemon, 1987). Although originally considered a low-angle normal fault (Ehlig, 1979), the roughly linear trace of the fault across the eastern boundary of the Capistrano Embayment suggests strike-slip character. Reverse drag inferred to represent listric (concave, flattening with depth) faulting may be due to the southwest curvature of the fault trace at the coastal bluff. Furthermore, reverse drag character observed in folded hanging wall sediments above the normal separation fault may be produced by structural inversion of the hanging wall basin due to a tectonic strain change from extension to contraction, or from transtension to transpression for strike-slip systems. Transtension during the Miocene microplate capture of the Western Transverse Ranges rifted the crustal block away from the continental margin by the northwest-translation of the Pacific oceanic plate. Subsequent changes in the relative plate motion vector and inland jump of the plate boundary to the Gulf of California produced a transpressional (oblique-convergence) regime within the southern California region west of the San Andreas fault and Salton Sea (Legg, 1991; Crouch and Suppe, 1993; Nicholson *et al.*, 1994).

SONGS is located within the Capistrano Embayment above the hanging wall of the west-dipping Cristianitos fault. The Cristianitos fault and fractures identified in the Tertiary (San Mateo Formation) bedrock foundation at Units 2 and 3 are considered inactive, by surface fault rupture standards (Alquist-Priolo). Notwithstanding, there are several small earthquakes (M3-4) recorded within the Capistrano Embayment, and some are located close to SONGS (Figures 2-5 and 2-8). Activity on the San Joaquin Hills (SJH) blind thrust (Mueller et al. 1998) may be responsible for some of these events, but uplift due to structural inversion above the Cristianitos fault is also feasible. Uplift or folding of the San Mateo Formation within the Capistrano Embayment during large (M>7) multi-fault earthquake ruptures may produce subsurface fractures on more brittle layers such as those observed in the coastal bluff near the fault. Grant et al (2002) presented evidence for a large coastal earthquake that produced uplift along the coast and in Newport Bay since A.D. 1635. The SJH was not modeled for the tsunami analysis because it lies onshore. The potential for shallow deformation at SONGS due to blind faulting in the Capistrano Embayment is uncertain at this time. The secondary fractures that could result from such events would not adversely affect the SONGS ISFSI, given its reinforced concrete slab support foundation and rigid construction.

2.3.2 Liquefaction

The NUHOMS ISFSI is underlain by the dense, well-consolidated sands of the San Mateo Formation, which are considered to be at low risk of seismically-induced liquefaction.

Strong shaking of water-saturated, cohesionless, surficial sediments may induce liquefication or liquefaction of the material. Pressure from the overlying intact material forces the liquefied material upward through cracks to form “sand blows” or sand volcanoes. Layers of liquefiable material buried beneath more cohesive soils including clays and hard-pan may create

cracks in the more cohesive material, and the entire soil sequence may slide laterally on very gentle slopes (lateral spread; Figure 2-8). In the North San Diego County area, there are numerous features that record prehistoric (and possibly historic) episodes of earthquake-induced liquefaction (Kuhn, 2005; Legg et al., 2018). Pre-WWII aerial photographs (1941) of the coastal area taken before the widespread development show features that resemble sand blows identified in the New Madrid, Missouri, area where a series of large earthquakes shook the Midwest in the winter of 1811-1812. (Obermeier, 1996). Although engineering geologists typically consider that only youthful cohesionless deposits are susceptible to liquefaction, that is, deposits older than 15,000 years are considered too dense to liquefy, there is abundant evidence of liquefaction events involving Pleistocene (MIS-5e terrace sands >125,000 years; Figure 2-8) and dense Eocene sands (Santiago Formation, 40-46 Million years; Kuhn, 2005) were found in the Carlsbad area. However, no liquefaction evidence of sands or silts within the Miocene San Mateo Formation have been identified through the scientific literature review for this report. Identification of fractures in the San Mateo Formation during excavation for Units 2 and 3 suggest brittle behavior, and slight cementation was observed, indicating that liquefaction of the soil beneath the ISFSI is unlikely.

While Quaternary deformation in the Capistrano Embayment remains poorly understood, it appears to be minor compared to the offshore deformation. Lack of offset above the wave-cut platform suggests little or no shallow fault deformation since about 125,000 years ago. However, at least 12 lateral spread events are documented (Kuhn, 2005) along Encinas Creek slopes (Figure 2-8, bottom left) within the overlying late Pleistocene soils (<125,000 years ago). These indications were previously considered in the 2015 CCC Staff Report for the UMAX ISFSI, which found that "although these features are suggestive, the Commission does not consider them indicative of a serious liquefaction hazard at the proposed project site."

Although the water table is shallow at the site (approximately +5 feet MLLW), cyclic triaxial tests, field density tests, and very high blow counts during standard penetrometer tests have shown that liquefaction is not expected to occur during a design basis earthquake (GEI 2015). Minimum factors-of-safety against liquefaction in the plant area have been calculated at 1.5 to 2.0.

In light of the high factor of safety evident in the site-specific studies, and in the absence of any recent scientific research to suggest anything to the contrary, the previous conclusion of the CCC Staff remains valid "that the stability of the site with respect to liquefaction can be assured, to the greatest extent feasible, consistent with section 30253 of the Coastal Act."

2.3.3 Slope Stability

This section summarizes studies estimating slope displacement that could result from ground shaking or common slope failure (SCE, 1995; Hinkle 2011; Nino and Moore, 2015) impacting the SONGS ISFSI. Figure 2-12 shows the locations of the two ISFSI facilities, referred to as "NUHOMS" for the eastern site housing Unit 1 material, and "Holtec-UMAX" for the western site containing material from Unit 2. The NUHOMS ISFSI for Unit 1 material was approved by the California Commission in February 2000. Ascending slopes are located at the north and east of the ISFSI sites.

The north and east slopes are about 105 ft and 200 ft away from the ISFSI, respectively. In the geotechnical investigation performed by SCE (1995), it was found that only minor sloughing of the surficial slope materials is likely to occur during the DBE-level ground shaking. Hinkle (2007) found that when conservatively assuming a slope failure during a design seismic or a tsunami event, the anticipated slope run-out distance of the adjacent slope is about 91 ft (Appendix A). When assuming a 20º to 25º angle of repose (from horizontal) for soils formed by the failed slope, a slope run-out distance of 50-70 ft is estimated. Therefore, any slope failures from the north bluff will be more than about 20 ft away from the ISFSI (Figure 2-12), and a much large distance away for east bluff failures.



Figure 2-12. Plan view of Holtec (west, lower) and NUHOMS (east, upper) ISFSIs. Minimum distance between the north and east bluffs is 105 ft.

2.3.4 Bearing Capacity

SCE constructed SONGS Units I, 2, and 3 in accordance with the seismic standards established by the Nuclear Regulatory Commission (NRC). The NRC performed a comprehensive evaluation of the soil properties and stability of the site foundation prior to issuing the operating licenses for these units, in part, for the purposes of assuring stability and structural integrity, and assuring that the units do not create or contribute to erosion or geologic instability of the surrounding area.

The static bearing pressure of the NUHOMS ISFSI is computed as 2,020 lb/ft^2. The allowable static bearing capacity of the soil was determined to be 15,630 lb/ft^2 (Appendix B). This is more than 7 times the required static bearing capacity.

The seismic soil pressure of the NUHOMS ISFSI, which considers the 1.5g horizontal and 1.0g vertical design ground stress, is computed as 6,670 lb/ft^2. The allowable bearing value can be increased by 50% for loads of short duration, including wind and seismic forces. Therefore, the allowable dynamic soil bearing capacity is approximately 23,400 lb/ft^2. This is more than three times the required dynamic bearing capacity. Appendix C presents the ISFSI Foundation Design calculations.

3.0 REFERENCES

Astiz, L. and Shearer, P.M., 2000. Earthquake locations in the inner Continental Borderland offshore southern California. *Seismological Society of America Bulletin, v. 90,* p. 425-449.

Atwater, T., 1970. Implications of plate tectonics for the Cenozoic evolution of western North America. *Geological Society of America Bulletin, v.81,* 3515-3536.

Atwater, T., and J. Stock, 1998. Pacific-North American plate tectonics of the Neogene southwestern United States: An update. *International Geology Review*, 40,375-402.

Barrows, A.G., 1974. A review of the geology and earthquake history of the Newport-Inglewood Structural Zone, southern California. California Division of Mines and Geology, Special Report 114, 115 pp.

Bohannon, R.G., and Geist, E., 1998. Upper crustal structure and Neogene tectonic development of the California Continental Borderland. *Geological Society of America Bulletin*, 110, 779-800.

Boore, D.M., and Atkinson, G.M., 2008, Ground-Motion prediction equations for the average horizontal component of PGA, PGV, and 5%-damped PSA at spectral periods between 0.01 s and 10.0 s: Earthquake Spectra, v. 24, n. 1, p. 99-138, Earthquake Engineering Research Institute.

Borrero, J.C., M.R. Legg, and C.E. Synolakis, 2004. Tsunami sources in the southern California bight. *Geophysical Research Letters*, v. 31, p. L13211.

Branum, D. S., Harmsen, E. K., M. Petersen and C Wills, 2008. Earthquake Shanking Potential for California, Map Sheet 48 (revised), California Geological Survey, Sacramento, California.

California Coastal Commission (CCC), 2015. Construct and operate an Independent Spent Fuel Storage Installation (ISFSI) to store spent nuclear fuel from SONGS Units 2 and 3. Staff Report: Regular Permit, Application #9-15-022, Approval with conditions, 47 pp., 2 Appendices, 9 Exhibits.

Clarke, S.H., Greene, H.G., Kennedy, M.P., and Vedder, J. G., 1987. Geologic map of the inner-southern California continental margin. California Division of Mines and Geology, California Continental Margin Geologic Map Series, Area 1 of 7, sheet 1 of 4, scale 1:250,000.

Clements, T., and Emery, K.O., 1947. Seismic activity and topography of the sea floor off southern California. Bulletin of the Seismological Society of America, v. 37, p. 309-313.

Coastal Environments, Inc. (CE), 2022. Tsunami Hazards Analysis at San Onofre Nuclear Generating Station, Report prepared for Southern California Edison, CE Reference No. 22-04, 82 pp.

Conrad, J.E., Brothers, D.S., Maier, K.L., Ryan, H.F., Dartnell, P., and Sliter, R.W., 2019. Right-lateral fault motion along the slope-basin transition, Gulf of Santa Catalina, Southern California. In Marsaglia, K.M., Schwalbach, J.R., and Behl, R.J., *From the Mountains to the Abyss: The California Borderland as an Archive of Southern California Geologic Evolution*. SEPM Special Publication No. 110, p. 256-272. Doi: 10.2110/sepmsp.110.07.

Crouch, J.K., and Suppe, J., 1993. Late Cenozoic tectonic evolution of the Los Angeles basin and inner California borderland: A model for core complex-like crustal extension. *Geological Society of America Bulletin*, 105, 1415-1434.

Crowell, J.C., 1974. Origin of late Cenozoic basins in southern California. In Dickinson, W. R., ed., *Tectonics and Sedimentation*. Society of Economic Paleontologists and Mineralogists Special Publication 22, 190-204.

Dartnell, P., Driscoll, N.W., Brothers, D., Conrad, J.E., Kluesner, J., Kent, G., and Andrews, B., 2015. Colored shaded-relief bathymetry, acoustic backscatter, and selected perspective views of the inner continental borderland, Southern California, U.S. Geological Survey Scientific Investigations Map 3324, 3 sheets https://dx.doi.org/10.3133/sim3324.

Ehlig, P.L., 1979. The late Cenozoic evolution of the Capistrano Embayment. In D. L. Fife, ed., Geologic guide of San Onofre nuclear generating station and adjacent regions of southern California: Pacific Sections. AAPG-SEPM-Society of Exploration Geophysicists, Guide Book 46, p. A38-A46.

Emery, K.O., 1960. *The Sea Off Southern California, A Modern Habitat of Petroleum*. John Wiley & Sons, Inc., New York, New York, 366 p.

Fischer, P.J., and Mills, G.I., 1991. The offshore Newport-Inglewood-Rose Canyon Fault zone, California: Structure, segmentation and tectonics. In Abbott, P. L., and Elliott, W. J., eds., *Environmental Perils San Diego Region*. San Diego Association of Geologists, p. 17-36.

Fletcher, J.M., Teran, O.J., Rockwell, T.K., Oskin, M.E., Hudnut, K.W., Spelz, R.M., Lacan, P. Dorsey, M.T., Ostermeijer, G., Mitchell, T.M., Akciz, S.O, Hernandez-Flores, A.P., Hinojosa-Corona, A., Pena-Villa, I., and Lynch, D.K., 2020. An analysis of the factors that control fault zone architecture and the importance of fault orientation relative to regional stress. *Geological Society of America Bulletin*, September/October v. 132, no. 9/10, p. 2084-2104.

GeoPentech, 2010. San Onofre Nuclear Generating Station Seismic Hazard Assessment Program 2010 Probabilistic Seismic Hazard Analysis Report. Prepared for Southern California Edison, December 2010.

Grant, L.B., and Rockwell, T.K., 2002. A northward-propagating earthquake sequence in coastal California? *Seismological Research Letters*, v. 73, n. 4, p. 461-469.

Grant, L.B., Ballenger, L.J., and Runnerstrom, E.E., 2002. Coastal uplift of the San Joaquin Hills, southern Los Angeles Basin, California, by a large earthquake since 1635 A.D. *Bulletin of the Seismological Society of America*, v. 92, p. 590-599.

Grant, L.B., and Shearer, P.M., 2004. Activity of the offshore Newport- Inglewood Rose Canyon Fault Zone, coastal southern California, from relocated microseismicity. *Bulletin of the Seismological Society of America, v.* 94, no. 2, p. 747- 752.

Hammling, I.J., Hreinsdóttir, Clark, K., and 23 others, 2017. Complex multifault rupture during the 2016 M_w 7.8 Kaikōura earthquake, New Zealand. *Science*, doi:10.1126/ science.aaam7194.

Hauksson, E., and Jones, L.M., 1988. The July 1986 Oceanside (M_L=5.3) earthquake sequence in the continental borderland, southern California. *Seismological Society of America Bulletin*, v. 78, p. 1885-1906.

Hauksson, E., and S. Gross, 1991. Source parameters of the 1933 Long Beach earthquake. *Bull. Seis. Soc. Am., 81*, 81-98.

Hauksson, E., 2000. Crustal structure and seismicity distribution adjacent to the Pacific and North America plate boundary I southern California. *Journal of Geophysical Research*, v. 105, no. B6, p. 13,875-13,903.

Hauksson, E., W. Yang, and P.M. Shearer, 2012. Waveform relocated earthquake catalog for southern California (1981 to June 2011). *Bull. Seis. Soc. Am* (short note), *102*(5), 2239–2244, doi: 10.1785/0120120010.

Hinkle, D., 2011. Third-Party Review – Slope Evaluation, Independent Spent Fuel Storage Installation (ISFSI), San Onofre Nuclear Generating Station: dated 17 May, 2011.

Holmes, J.J., Perea, H., Driscoll, N.W., and Kent, G.M., 2021. Revealing geometry and fault interaction on a complex structural system based on 3D-Cable data: The San Mateo and San Onofre trends, offshore Southern California. *Frontiers in Earth Science*, 9:653366 doi:10.3389/feart.2021.653366.

Holtec International, 2015. 2001 CDP Permit Structural Calculations: dated 19 February 2015.

Hutton, K., J. Woessner, and E. Hauksson, 2010. Earthquake monitoring in southern California for seventy-seven years (1932-2008). *Bull. Seis. Soc. Am., 100*, 423-446.

Jennings, C.W., 1994. Fault activity map of California and adjacent areas. California Division of Mines and Geology, Map No. 6, scale 1:750,000.

Joyner, W.B., and Boore, D.M., 1993, Methods for regression analysis of strong-motion data: Bull. Seismol. Soc. Am., v. 83, p. 469-487.

Kennedy, M.P., 1977. Recency and character of faulting along the Elsinore fault zone in southern Riverside County, California. California Division of Mines & Geology Special Report 131, 12 p. Map scale 1:24,000.

Kramer, S.L., 1996. *Geotechnical Earthquake Engineering.* Prentice Hall, Upper Saddle River, New Jersey, 653 p.

Langenheim, V.E., P.F. Halvorson, E.L Castellanos, and R.C. Jachens, 1993. Aeromagnetic Map of the Southern California Borderland East of the Patton Escarpment, U.S. Geol. Survey. Open-File Rept. 93-250, scale 1:500,000.

Legg, M.R., 1980. Seismicity and tectonics of the inner continental borderland of southern California and northern Baja California, Mexico [unpublished M.S. thesis]: University of California, Santa Diego, San Diego, California, 60 p.

Legg, M.R., 1985. *Geologic Structure and tectonics of the inner continental borderland offshore northern Baja California, Mexico*. [Ph.D. dissertation] University of California, Santa Barbara, Santa Barbara, California, 410 p.

Legg, M.R., 1987. Earthquake epicenters and selected fault plane solutions of the inner-southern California continental margin. Map No. 1B in Greene, H.G., and M.P. Kennedy, eds., Geologic Map Series of the California Continental Margin, Calif. Div. Mines & Geology, Area 1 of 7 (NOS 1206N-16), Scale 1:250,000 (also 3B).

Legg, M.R., 1991. Developments in understanding the tectonic evolution of the California Continental Borderland. In Osborne, R. H. ed., *From Shoreline to Abyss,* SEPM Shepard Commemorative Volume, 46, 291-312.

Legg, M.R., 2021. Develop Geological Model of Offshore Southern California (Borderland) for the Community Rheology Model: Southern California Earthquake Center (SCEC5) Project Report #20117.

Legg, M.R., Wong-Ortega, V., and Suarez-Vidal, F., 1991. Geologic structure and tectonics of the inner continental borderland of northern Baja California. In Dauphin, P., and G. Ness, editors, *The Gulf and Peninsular province of the Californias:* American Association of Petroleum Geologists *Memoir #47*, p. 145-177.

Legg, M.R., and Goldfinger, Chris, 2002. Earthquake potential of major faults offshore southern California: Collaborative research with Oregon State University and Legg Geophysical, Final Technical Report, U.S. Geological Survey Grant No. 01HQGR0017, 24 p.

Legg, M.R., J.C. Borrero, and C.E. Synolakis, 2004. Tsunami hazards associated with the Catalina fault in southern California. *Earthquake Spectra*, vol. 20, p. 917 -950.

Legg, M.R., C. Goldfinger, M.J. Kamerling, J.D. Chaytor, and D.E. Einstein, 2007. Morphology, structure and evolution of California Continental Borderland restraining bends. In Cunningham, W.D. & Mann, P. (eds), *Tectonics of strike-slip restraining & releasing*

bends in continental and oceanic settings, Geological Society of London Special Publications, v. 290, p. 143-168.

Legg, M.R., M.D. Kohler, N. Shintaku, and D.S. Weeraratne, 2015. High-resolution mapping of two large-scale transpressional fault zones in the California Continental Borderland: Santa Cruz-Catalina Ridge and Ferrelo. *Journal of Geophysical Research*: Earth Surface, vol. 120, doi:10.1002/2014JF003322.

Legg, M., C. Sorlien, C. Nicholson, M. Kamerling, and G. Kuhn, 2018. Potential for large complex multi-fault earthquakes offshore southern California. *Proceedings Eleventh U.S. National Conference on Earthquake Engineering*, Los Angeles, CA.

Maloney, J.M., Driscoll, N.W., Kent, G.M., Duke, S., Freeman, T., and Bormann, J.M., 2016. Segmentation and stepovers along strike-slip fault systems in the Inner California Borderlands: Implications for fault architecture and basin formation. In Anderson R., and Ferriz, H., eds., *Applied Geology in California*, Association of Environmental and Engineering Geologists, Special Publication Number 26, Chapter 36, p. 655-677, Star Publishing Company, Redwood, California.

Mueller, K.J., Grant, L.B., and Gath, E., 1998. Late Quaternary growth of the San Joaquin Hills anticline a – new source of blind thrust earthquakes in the Los Angeles basin [abstract]. Seismological Society of America 1998 Annual Meeting, *Seismological Research Letters*, v. 69, no.2, P. 161-162.

National Archive of Marine Seismic Surveys (NAMSS), 2006. http://walrus.wr.usgs.gov/NAMSS/

Nicholson, C., and J.K. Crouch, 1989. Neotectonic structures along the central and southern California margin: Predominantly a thrust regime? *Seis. Res. Letters, 60,* 23-24.

Ninyo & Moore, 2015. SONGS ISFI Slope Calculations: Report submitted to Southern California Edison, dated 16 April 2015.

Pacheco, J., and Nabelek, J., 1988. Source mechanisms of three moderate California earthquakes of July 1986. *Seismological Society of America Bulletin*, v. 78, p. 1907-1929.

Plesch, A., Shaw, J.H., Benson, C., Bryant, W.A., Carena, S., Cooke, M., Dolan, J., Fuis, G., Gath, E., Grant, L., Hauksson, E., Jordan, T., Kamerling, M., Legg, M., Lindvall, S., Magistrale, H., Nicholson, C., Niemi, N., Oskin, M., Perry, S., Planansky, G., Rockwell, T., Shearer, P., Sorlien, C., Suss, M.P., Suppe, J., Treiman, J., and Yeats, R., 2007. Community Fault Model (CFM) for southern California. *Bulletin Seismological Society of America*, v. 97, p. 1793-1802, DOI: 10.1785/0120050211.

Rivero, C., Shaw, J.H., and Mueller, K., 2000. Oceanside and Thirtymile Bank blind thrusts: Implications for earthquake hazards in coastal southern California. *Geology*, v. 28, p. 891-894.

Rivero, C., and Shaw, J. H., 2011. Active folding and blind-thrust faulting induced by basin inversion processes, Inner California Borderlands. In McClay, K., Shaw, J., and Suppe, J., eds., *Thrust fault-related folding,* AAPG Memoir 94, p. 187-214.

Ryan, H.F., Legg, M.R., Conrad, J.E., and Sliter, R.W., 2009. Recent faulting in the Gulf of Santa Catalina; San Diego to Dana Point; Earth science in the urban ocean; the Southern California continental borderland. In Lee, H.J., and Normark, W.R., eds., *Earth Science in the Urban Ocean—The Southern California Continental Borderland.* Geological Society of America Special Paper v. 454, p. 291-315, doi:10.1130/2009.2454(4.2)

Ryan, H.F., J.E. Conrad, C.K. Paull, and M. McGann, 2012. Slip rate on the San Diego Trough fault zone, Inner California Borderland, and the 1986 Oceanside earthquake swarm revisited. *Seis. Soc. Am. Bull*, *102*, 2300-2312.

Sahakian, V., Bormann, J., Driscoll, N., Harding, A., Kent, G., and Wesnousky, S., 2017. Seismic constraints on the architecture of the Newport-Inglewood/Rose Canyon fault: Implications for the length and magnitude of future earthquake ruptures. *Journal of Geophysical Research Solid Earth*, v. 122, p. 2085-2105. Doi: 10.102/2016JB013467.

Shepard, F.P., and Emery, K.O., 1941. Submarine topography off the southern California coast: Canyons and tectonic. *Geological Society of America, Special Paper 31*, 171 p.

Shlemon, R.J., 1987. *The Cristianitos fault and Quaternary geology, San Onofre State Beach, California. Geological Society of America Centennial Field Guide – Cordillera Section*, p. 171-174.

Sorlien, C.C., J.T. Bennett, M.-H. Cormier, B.A. Campbell, C. Nicholson, and R. L. Bauer, 2016. Late-Miocene-Quaternary fault evolution and interaction in the southern California Inner Continental Borderland. *Geosphere, v. 11,* p. 1111-1132, doi:10.1130/GES01118.1.

Southern California Edison Company, 1995. Final Report, Geotechnical Investigation of Yee, Torrey, 2001. Calculation of Ultimate Bearing Capacity, Exhibit 14, E-00-014, dated February 15.

Sylvester, A.G., 1984. Wrench Fault Tectonics: Selected papers reprinted from the AAPG Bulletin and other geological journals, *AAPG Reprint Series* No. 28, 374 pp.

Thompson, M., and Francis, R.D., 2019. Tectonic evolution of the Palos Verdes fault-Lasuen Knoll segment, offshore southern California. In Marsaglia, K.M., Schwalbach, J.R., and Behl, R.J., eds., *From the Mountains to the Abyss: The California Borderland as an archive of Southern California Geologic Evolution*. SEPM Special Publication No. 110, p. 241-255. Doi: 10.2110/sepmsp.110.17.

Yee, Torrey, 2001, Calculation of Ultimate Bearing Capacity, Exhibit 14, E-00-014, datedFebruary 15.

U.S. Geological Survey and California Geological Survey. Quaternary fault and fold database for the United States, accessed February 2, 2020, at: https://www.usgs.gov/natural-hazards/earthquake-hazards/faults.

Vedder, J.G., Beyer, L.A., Junger, Arne, Moore, G.W., Roberts, A.E., Taylor, J.C., and Wagner, H.C., 1974. *Preliminary report on the geology of the Continental Borderland of southern California*. U.S. Geological Survey, Miscellaneous Field Studies *Map MF-624*, Scale 1:500,000.

Wallace, R.E., 1990. *The San Andreas Fault System, California*. U.S. Geological Survey Professional Paper 1515, 283 pp.

Wilcox, R.E., Harding, T.P., and Seeley, D.R., 1973. Basic wrench tectonics. *American Association of Petroleum Geologists Bulletin*, 57, 74-96.

APPENDIX A

SONGS ISFSI
SLOPE STABILITY

Dale Hinkle P.E., PLLC
P.O. Box 1016
Bonner, MT 59823
(406)244-0498
e-mail: hinklepe@gmail.com

CA RGE# 402
CARCE# 23023
MT PE#14041

Federal I.D.
45-2139130

May 27, 2011

Mr. Zaid Ahmad
Southern California Edison Company
300 North Lone Hill
San Dimas, CA 91773

Dear Mr. Ahmad:

Re: Third Party Review – Slope Evaluation
Independent Spent Fuel Storage Installation (ISFSI)
San Onofre Nuclear Generating Station

At your request, I have performed a third party review of the two reports describing the uphill slope stability (seismic case) for the above-referenced facility. The two reports are listed in the Appendix. They consist of a November, 1995 report issued by the SCE Geotechnical Group and an August 3, 2007 report/notice of calculation change by SCE Site Engineer, L. Pham. The difference in the studies is that the original 1995 study did not consider the 15-foot wide slope bench above the storage site. The 2007 study concluded that the maximum slope failure could reach 91 feet out from the existing toe of the ½:1 (horizontal to vertical) cut slope instead of 120 feet as mentioned in the 1995 report.

Observations

1. My review of the studies found their sources of data and assumptions were very similar. Both used Woodward-Clyde soil slope conditions and strengths. They are simply differences in judgment of the persons.

2. The sections analyzed (A-A' through D-D') were not shown on a plan by either report. I assume that the section modeled is on the north side of the facility where they show a 105 foot setback. This would be approximately 150 feet west of the north guard tower. It is interesting that Woodward-Clyde Sections A and B both showed the 15-foot bench and it was used in original stability calculations but was not used in the toe run-out calculations.

3. The failed slope profile was arbitrarily assumed in 1995 to be one-half the height of the original slope. The 2007 study used the same assumption. Both studies assumed a 15° lower failed slope angle. These assumptions are very arbitrary and very conservative.

The 1995 report indicated in Section 4.3 four profiles (A-A' through D-D') which were considered to be representative of the most critical slope geometry and closeness to the cask storage sides. These cross sections are missing in the report.

The angle of repose of the combined terrace soil would be in the 20° to 30° range. If we modeled the failure using a worst-case 20° to 25° slope, the toe run-out would be 50 to 70 feet. The value calculated is 91 feet and the available space is 105 feet. The setback of 105 feet is exceedingly conservative.

Conclusions

Based on my review of the two above-mentioned reports and my independent calculations of the setback using STABL7, and using the same assumptions as the 2007 report, I found a slope run-out of 92 feet which is almost identical to the original findings.

The arbitrary assumption that the failed slope would be half as high as the original is very conservative. The angle of repose for the soils formed by failed terrace would give a slope of at least 20° to 25° (not 15°) and would yield a toe run out of 50 to 70 feet.

Using the 15-foot wide mid-slope bench is the correct procedure and the 91 foot slope run-out is very conservative.

We appreciate the opportunity to be of service to you on this project. If you have any questions, please call our office.
Sincerely,



R. D. Hinkle
RGE #402

Attachments

APPENDIX B

ISFSI FOUNDATION DESIGN

CALCULATION TITLE PAGE

ECN NO./ PRELIM. CCN NO.	PAGE ____ OF ____

Calc. No. C-296-01.04 ECP No. & Rev. 061000254-2 , REV. 0

Subject ISFSI FOUNDATION DESIGN Sheet 1 of ____

System Number/Primary Station System Designator 2208/XDC SONGS Unit 1, 2&3 Q-Class II

Tech. Spec./LCS Affecting? ☒ NO ☐ YES, Section No. ____ Equipment Tag No. S1232208AHSM001

Site Programs/Procedure Impact? ☒ NO ☐ YES, AR No. ____

10CFR50.59/72.48 REVIEW	CONTROLLED COMPUTER PROGRAM / DATABASE		
IS THIS CALCULATION REVISION BEING ISSUED SOLELY TO INCORPORATE CCNs/ECNs? ☒ NO ☐ YES AR No. 010901113	☐ PROGRAM ☐ DATABASE N/A ACCORDING TO SO123-XXIV-5.1	PROGRAM / DATABASE NAME(S) ☐ ALSO, LISTED BELOW N/A	VERSION / RELEASE NO.(S) N/A

RECORDS OF ISSUES

REV. / DISC.	DESCRIPTION	TOTAL SHTS. / LAST SHT.	PREPARED BY: (Print name/sign/date) Initial PQS Block - Requires PQS T3EN64	APPROVED BY: (Signature/date) Initial PQS Block - Requires PQS T3EN64
3	Revised sheets: Cross index, 5, 10 & 12. Replaced sheets: 8, 9, 10 Added sheets: 34 thru 37	37	ORIG. L.PHAM PQS VER. BY: LP luanpham 5/17/07	FLS PQS VER. BY: RLP 8/10/07
CIVIL		37	IRE T. YEE PQS VER. BY: TY Tonee Yee 8/3/07	Other
			ORIG. PQS VER. BY: ____	FLS PQS VER. BY: ____
			IRE PQS VER. BY: ____	Other
			ORIG. PQS VER. BY: ____	FLS PQS VER. BY: ____
			IRE PQS VER. BY: ____	Other
			ORIG. PQS VER. BY: ____	FLS PQS VER. BY: ____
			IRE PQS VER. BY: ____	Other

Space for RPE Stamp, identify use of an alternate calc., and notes as applicable.



Poor Quality Document
Best Available Copy
Signed: luanpham 8/15/07
Document Originator Date

SITE FILE COPY

This calc. was prepared for the identified ECP. ECP completion and turnover acceptance to be verified by receipt of ECP Turnover/Closure form directing conversion. Upon receipt, this calc. represents the as-built condition. ECP Turnover/Closure form date ____ by ____.

Site File Copy

CALCULATION CROSS-INDEX

ICCN NO./ PRELIM. CCN NO.	PAGE ____ OF ____
	CCN CONVERSION: CCN NO. CCN-

Calculation No. C-296 - 01.04 Sheet No. 2 of ____

Calc. rev. number and responsible FLS initials and date	INPUTS: These interfacing calculations and/or documents provide input to the subject calculation and if revised may require revision of the subject calculation.		OUTPUTS: Results and conclusions of the subject calculation are used in these interfacing calculations and/or documents.		Does the output interface calc/ document require change?	Identify output interface calc/document CCN, DCN, TCN/Rev., FIDCN, or tracking number.
	Calc / Document No.	Rev. No.	Calc / Document No.	Rev. No.	YES / NO	
0 SY 6-4-01	S01-207-1-C11 C-296-1.01 C-296-01.02 S01-207-1-M135	5 0 0 0	28010	0	No	
1 4/5/02			28002	0	No	
2 3/26/03	S01-207-1-D173 S-02-C-001	0 0			No	
3 8/10/07	S023-207-16-D109	0	28002	1	YES	ECN A46647

SCE 26-424 REV. 3 8/99 [REFERENCE: SO123-XXIV-7.15]

EC&FS DEPARTMENT

CALCULATION SHEET

ICCN NO./ C-1	PAGE ___ OF ___
PRELIM. CCN NO.	
CCN CONVERSION: CCN NO. CCN -	

Project or DCP/FCN **SONGS 1** Calc No. **C-296-01.04**

Subject **ISFSI Foundation Design** Sheet 3 of ___

REV	ORIGINATOR	DATE	IRE	DATE	REV	ORIGINATOR	DATE	IRE	DATE
0	H. Hadidi HH	3/12/01	J. Wang	5/3/01					
3			T. Yee	7/31/07					

REV INDICATOR

TABLE OF CONTENTS

		SHEET
1.	Introduction / Purpose	4
2.	Results / Conclusions	4
3.	Assumptions	4
4.	Design Inputs	5
5.	Methodology	5
6.	References	6
7.	Nomenclature	6
8.	Calculations	7
	• ISFSI FOUNDATION FOR SINGLE ROW OF MODULES	7
	• SLAB ON GRADE FOR DRY CASK TRANSPORTATION	11
	• CONCRETE PAD TARGET HARDNESS	27
	• PAD INSPECTION	33
	• ISFSI FOUNDATION FOR BACK TO BACK MODULES	34

EC&FS DEPARTMENT

CALCULATION SHEET

ICCN NO./ C-1 PRELIM. CCN NO.	PAGE ___ OF ___
CCN CONVERSION: CCN NO. CCN -	

Project or DCP/FCN **SONGS 1** Calc No. **C-296-01.04**

Subject **ISFSI Foundation Design** Sheet 4 of ____

REV	ORIGINATOR	DATE	IRE	DATE	REV	ORIGINATOR	DATE	IRE	DATE
0	H. Hadidi HH	5/11/01	J Wang	5/31/01					
2	T. YEE SY	3/4/03	DC Gwin	3/24/03					

REV INDICATOR

1. Introduction / Purpose

The purpose of this calculation is to design the reinforced concrete pad for the storage modules of Independent Spent Fuel Storage Installation (ISFSI). There are multiple storage modules placed on the concrete pad and they are connected together to form a single structure.

The purpose of this calculation is also to design the slab-on-grade adjacent to the ISFSI pad. The design of a concrete vault that would provide access to an existing man-hole (that will be completely covered by the pad) is included in this calculation for information only. Current design does not include this vault since access to the manhole is not required.

The Pad's Target Hardness is calculated for cask drops. Baseline inspections of the pad are included in this calc. (2)

2. Results / Conclusions

Design loads are based on seismic accelerations of 1.5g horizontal and 1.0g vertical.

ISFSI concrete pad : 3'-0 thick
Moment (Capacity) = 322 foot kips > Moment (Design Load) = 260 ft kips
Allowable Soil Bearing = 23.5 ksf >Soil Bearing (Design) = 10.11 ksf

Slab-on-grade : 1'-0 thick
Jack load (Capacity) = 106.7 kips > Jack load (Design) = 105.6 kips
Punching shear (Capacity) = 334 kips >Jack load (Design) = 105.6 kips
Capacities based on S. F. of 1.6 and base plate size of 29"x29".

Existing manhole top plate : 1-3/4" thick steel plate
Moment (Capacity) = 41.3 ft kips > Moment (Design Load) = 36.34 ft kips

Existing manhole: Bearing capacity = 6,807 kips > Bearing load = 595 kips

~~3. Assumptions - Stated in calculation.~~

Pad Target Hardness: $S = 83{,}697 < 400{,}000$

Concrete cracks are classified as "hairline", except for one crack which is a "fine crack." All cracks are acceptable. (2)

3. Assumptions – Stated in calculation.

REV	ORIGINATOR	DATE	IRE	DATE	REV	ORIGINATOR	DATE	IRE	DATE
0	H. Hadidi HH	5/11/01	J. Wang	5/21/01					
3	L. PHAM	5/06/07	T. Yee	8/3/07					

REV INDICATOR

4. Design Inputs

Module weight = 400 + 70 = 470 kips with back wall (Ref. 6.1, Table H1 and page H9). Used 471 kips in this calculation which is conservative.

Concrete compressive strength = 4000 psi; Fy = 60 ksi for A615, Grade 60

Seismic load: DBE 1.5g horizontal and 1.0g vertical (Reference TN West design spectra included in C-296-1.01, Rev. 0). SONGS requirements are actually based on a 0.67g seismic event. ~~The higher seismic accelerations were conservatively used to be consistent with the TN West design.~~ DUE TO THE MODULES SLIDING, THE HORIZONTAL ACCELERATION WILL BE 1.0g WHEN ASSUMING THE COEFFICIENT OF FRICTION HAS AN UPPER LIMIT OF 0.7. BY CONSIDERING SLIDING, THE VERTICAL ACCELERATION WILL ALSO BE LIMITED TO 0.44g. THEREFORE, THE TOTAL VERTICAL FORCE OF (DL+0.44g).0.7 = 1.0g FOR HORIZONTAL DIRECTION

3

5. Methodology

The multiple storage modules are placed in a single row without any separation between them. The modules are not anchored to the concrete pad.

Soil pressure is calculated by using a two-component horizontal seismic load of ~~1.5g~~ 1.0g and a vertical component of 1.0 g, and combining them by SRSS method. The reinforcing design is based on the moment calculated for a 10 feet cantilever one-way slab, loaded with the resultant of maximum soil pressure. Reinforced concrete design is in accordance with ACI 349.

3

The structural design and stability of the storage module are given in Ref. 6.4.

The concrete vault walls are designed to resist the loads before and after the construction of the ISFSI pad. The walls are considered to be cantilever before pad construction and simply supported after the pad construction. The bottom slab of the vault is designed to resist the soil pressures due to the dead and live loads. The steel plate covering the vault is designed for 3' of soil on top of the plate plus a truck wheel load of 16 kips.

The slab-on-grade is designed for both the transporter truck wheel loads and the jack loads corresponding to the loading of the spent fuel cask into the modules.

REV	ORIGINATOR	DATE	IRE	DATE	REV	ORIGINATOR	DATE	IRE	DATE
0	H. Hadidi HH	5/11/01	J. Wang	5/31/01	2	T. Yee	3/4/03	QE	3/24/03
1	T. Yee	4/3/02	QE	4/5/02					

REV INDICATOR

6. References (See Sheets 27 & 32 for additional references) 2

6.1 SO1-207-1-C11, Rev. 5, DSC/AHSM/0S197 Cask Component Weights, Mass Properties, and Lift Weight Calculation and Evaluation by TN West.

6.2 SCE Calculation C-296-1.01, Rev. 0, Seismic Response of ISFSI Pad.

6.3 ACI Manual Of Concrete Practice-Code Requirements for Nuclear Safety Related Concrete Structures (ACI-349).

6.4 SO1-207-1-M135, Rev. ~~0~~ 2, Safety Analysis Report for the Standardized Advanced NUHOMS Horizontal Modular Storage System for Irradiated Nuclear Fuel, by TN West. 2

6.5 SONGS 2&3 Preliminary Safety Analysis Report, Appendix 2B, Seismic and Foundation Studies for Proposed Units 2 and 3, San Onofre Nuclear Generating Station - Dames and Moore.

6.6 Designing Floor Slabs on Grade Design Manual, Second Edition.

6.7 SCE Calculation C-296-01.02, Rev. 0, ISFSI Pad Other Events Hazard Evaluation.

6.8 S01-207-1-M19, Rev. 2.

6.9 Bowles, J. E., "Foundation Analysis and Design," Third Edition.

6.10 Gaylord and Gaylord, "Structural Engineering Handbook," Second Edition.

6.11 SONGS 2&3 UFSAR, Appendix 3.7C, Soil-Structure Interaction Parameters, Woodward-McNeill. 1

7. Nomenclature

ISFSI - Independent Spent Fuel Storage Installation
AHSM - Advanced Horizontal Storage Module
TNW - TransNuclear West
SRSS- Square Root of the Summation of Squares
g - Acceleration of Gravity
q - Soil pressure

CALCULATION SHEET

PRELIM. CCN NO. PAGE

CCN CONVERSION:
CCN NO. CCN-

Project or DCP/FCN _____ Calc No. C-296-01.04

Subject ISFSI FOUNDATION DESIGN Sheet 7 of

REV	ORIGINATOR	DATE	IRE	DATE	REV	ORIGINATOR	DATE	IRE	DATE
0	HASSAN HADIA	3/12/01	J. Wong	5/31/01					

REV INDICATOR

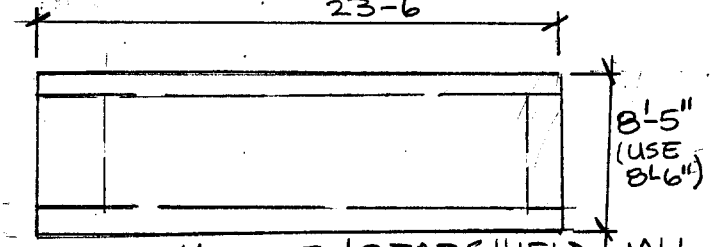
8.0 CALCULATIONS

ISFSI FOUNDATION DESIGN:

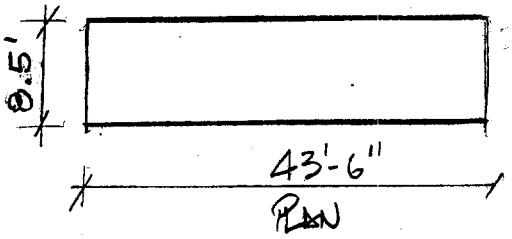
MODULE WEIGHT = 400K → FOR REFERENCE SOI-207-1-C11, TABLE H1

PAD SIZE FOR A SINGLE MODULE

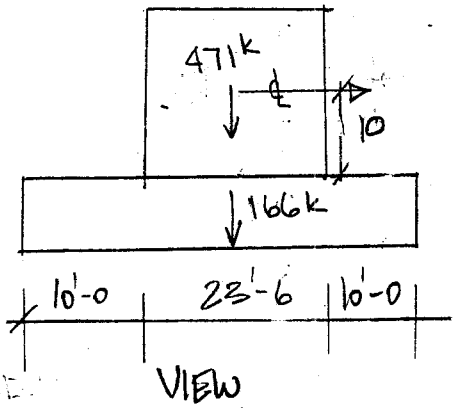
USE 43.5' x 8.5' x 3.0'
(REF. 6.1)



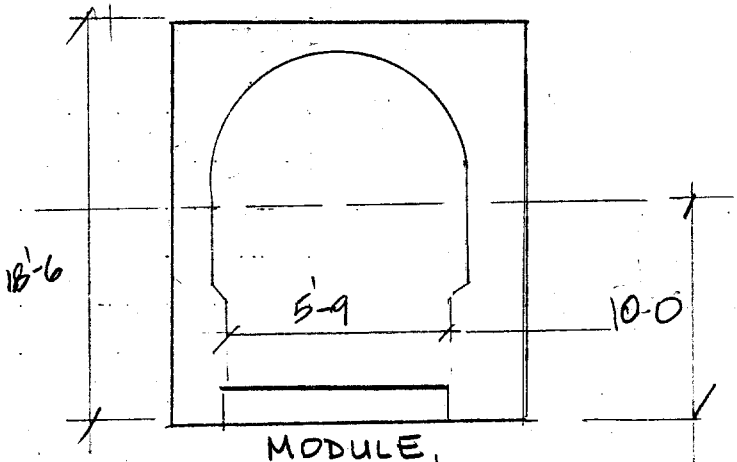
MODULE & REAR SHIELD WALL PLAN



PLAN



VIEW



MODULE SECTION

REAR SHIELDING WALL WT:

18.5 x 3 x 8.5 = 71k

TOTAL MODULE WT. = 400 + 71 = 471k
(INCLUDING REAR SHIELD WALL)

WEIGHT OF PDN = 43.5 x 3 x 8.5 x .15 = 166k

∴ Σ_W = 471 + 166 = 637k MODULE + PAD

E&TS DEPARTMENT

CALCULATION SHEET

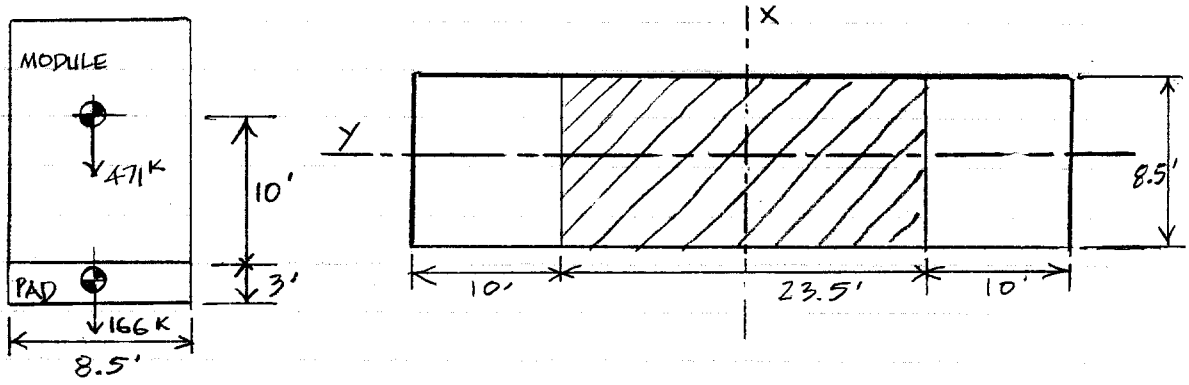
ECN NO./ PRELIM. CCN NO.	PAGE ____ OF ____
	CCN CONVERSION: CCN NO. CCN -

Project or ECP 061000254-2 Calc No. C-296-01.04

Subject ISFSI FOUNDATION DESIGN Sheet 8 of ____

REV	ORIGINATOR	DATE	IRE	DATE	REV	ORIGINATOR	DATE	IRE	DATE	REV INDICATOR
3	L. Pham		T. Yee	8/3/07						

CHECK SOIL PRESSURE DUE TO SEISMIC & DEAD WEIGHT OF MODULES



DEADLOAD SOIL PRESURE: $q_{DL} = \frac{V}{A} = \frac{471+166}{8.5 \times 43.5} = 1.72$ KSF

SEISMIC ACCELERATIONS:

SINCE THE MODULES ARE NOT ATTACHED TO THE PAD, THE HORIZONTAL ACCELERATION OF 1g IS USED IN DESIGN OF THE PAD

VERTICAL SEISMIC ACCEL. OF 0.44g IS USED WITH M=0.7 TO GET 1g HORIZONTAL. IT SHOULD BE NOTED THAT THE HORIZONTAL SEISMIC ACCERATION OF 1.5g HAS BEEN SHOWN TO DEVELOP @ THE C.G OF THE MODULE PER C-296-01.01 HOWEVER, THIS EXCESSIVE ACCELERATION IS DUE TO THE FACT THAT THE MODULES WERE MODELED AS RIGIDLY CONNECTED TO THE PAD. IN THE ANALYSIS, IN ALLOWING SLIDING THE HORZ. ACCELERATION IS 1.0g WHEN THE VERTICAL ACCELERATION IS 0.44g (SONGS DBE). THE VERT. ACCELERATION OF 1.0g WILL BE USED IN DESIGN.

SEISMIC SOIL PRESSURE ABOUT X-X:

$OTM_x = 1.0g \times 471 \times 13 + 1.5g \times 166 \times 1.5 = 6497$ K-FT

$e_x = \frac{OTM}{V} = \frac{6497}{637} = 10.2' > \frac{L}{6} = \frac{43.5}{6} = 7.25'$

$q_x = \frac{2V}{3B(\frac{L}{2} - e)} = \frac{2 \times 637}{3(8.5)(\frac{43.5}{2} - 10.2)} = 4.326$ KSF

SEISMIC SOIL PRESSURE ABOUT Y-Y

SINCE THE MODULES ARE TIED TOGETHER, THE SOIL PRESSURE WILL BE BASED ON 10 MODULES. ACTUALLY, 19 MODULES ARE PLANNED FOR SONGS 1

$OTM_Y = 10[1.0\times471\times13 + 1.5\times166\times1.5] = 64945$ K-FT

$e_y = \frac{64965}{10\times637} = 10.2' < \frac{L}{6} = \frac{10\times8.5}{6} = 14.17'$

$q_y = \frac{Mc}{I} = \frac{64965\times(85/2)(12)}{43.5(85)^3} = 1.24$ KSF

TOTAL SOIL PRESSURE:

$q_{TOT} = q_{DL} + [q_x^2 + q_y^2 + q_z^2]^{1/2} = 1.72 + [4.33^2 + 1.24^2 + 1.72^2]^{1/2}$

$= 1.72 + 4.82 = 6.54$ KSF $< 15.63\times1.5 = 23.5$ KSF.

ALLOWABLE SOIL BEARING OF 3FT EMBEDMENT AND 50% INCREASE FOR SEISMIC LOAD (REF. 6.5). THIS IS CONSERVATIVE IN COMPARISON TO FIGURE 13 OF REF. 6.11 WHICH ALLOWS A NET ALLOWABLE BEARING CAPACITY OF $25 + \frac{1}{2}(b-3)$, WHERE B= FOOTING WIDTH.

CONCRETE DESIGN (ACI 349)

ASSUME 10' OF PAD FROM MODULE TO THE EDGE OF CANTILEVER.

$M_u = \frac{qL^2}{2} = \frac{(6.54-0.45)(10)^2}{2} = 304.5$ K.FT/FT

$K_u = \frac{M_u}{bd^2} = \frac{304.5\times12}{12\times32^2} = 0.297$ KSI

$\rho = \frac{0.85\times f'_c}{f_y}\left[1 - \sqrt{1 - \frac{2K_u}{\phi 0.85 f'_c}}\right] = \frac{0.85\times4}{60}\left[1 - \sqrt{1 - \frac{2(0.297)}{0.9\times0.85\times4}}\right]$

$\rho = 0.0058 < 0.018$ MAX, > 0.0033 MIN, $A_s = \rho bd = 0.0058(12)(32) = 2.226$ IN^2

USE #11 @ 8", $A_s = 1.56\times12/8 = 2.34$ IN^2 > 2.226 IN^2 REQ.

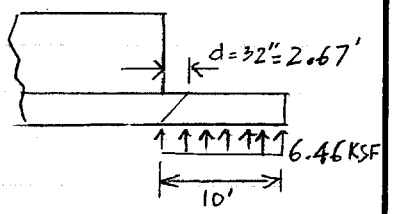
$V_u = (6.54-0.45)(10-2.67) = 44.64$ K/FT

$\phi V_c = \phi 2\sqrt{f'_c}\, bd = 0.75\times2\times\sqrt{4000}\times12\times32$

$= 36.43$ K/FT

$\phi V_s = V_u - \phi V_c = 44.64 - 36.43 = 8.2$ K/FT

$V_s = 8.2/0.75 = 10.95$ K/FT



E&TS DEPARTMENT

CALCULATION SHEET

ECN NO./ PRELIM. CCN NO.	PAGE ____ OF ____

CCN CONVERSION: CCN NO. CCN -

Project or ECP 061000254-2 Calc No. C-296-01.04

Subject ISFSI FOUNDATION DESIGN Sheet 10 of ____

REV	ORIGINATOR	DATE	IRE	DATE	REV	ORIGINATOR	DATE	IRE	DATE
3	L. Pham		T. Yee	8/3/07					

REV INDICATOR

TRT # 4 @ 12" ON CENTER $A_v = 0.2\ IN^2 > 50\frac{bs}{f_y} = \frac{50(12)(12)}{60,000} = 0.12\ IN^2$ (OK)

$$V_s = \frac{A_s f_y d}{S} = \frac{0.2(60)(32)}{12}$$

$V_s = 32\ K/FT > 10.95\ K/FT$ (OK)

$\frac{36.43}{6.54 - 0.45} = 5.98\ FT$ ∴ @ 5.98 FT FROM EDGE OF PAD

$V_u = 36.43\ K/FT = \phi V_c$ THUS, PROVIDE # 4 STIRRUP @ 12 IN SPACING FROM 4' TO 10' FROM EDGE OF PAD.

TEMPERATURE & SHRINKAGE REINFORCING STEEL IN LONGITUDINAL DIR.

$A_s = 0.0018 \times 12 \times 36 = 0.78\ IN^2/FT$

USE # 7 @ 12" TOP & BOTTOM $A_s = 1.2\ IN^2/FT > 0.78\ IN^2/FT$

FOR EAST WEST DIRECTION, USE #9 @ 12" O.C FOR TOP REINFORCING STEEL.

(SEE SHEET 34 FOR BACK TO BACK MODULE FOUNDATION DESIGN).

EC&FS DEPARTMENT

CALCULATION SHEET

ICCN NO./ PRELIM. CCN NO.	PAGE ____ OF ____
CCN CONVERSION: CCN NO. CCN -	

Project or DCP/FCN _____ Calc No. C-296-01.04

Subject ISFSI FOUNDATION DESIGN Sheet 11 of ____

REV	ORIGINATOR	DATE	IRE	DATE	REV	ORIGINATOR	DATE	IRE	DATE
0	HASSAN HADIDI HH	3/12/01	J. Wang	5/31/01					

REV INDICATOR

DESIGN OF SLAB ON GRADE FOR DRY CASK TRANSPORTATION [REF. 6.6]

MAX. TIRE PRESSURE = 130 PSI [REF. 6.8]

MAX LOAD PER TIRE = 8250# [" "]

TIRE AREA = $8250/130$ = 64 sq in

FLEXURAL STRENGTH OF CONCRETE $MR = 9\sqrt{f'c}$ = 569 psi

SLAB STRESS PER 1000# OF AXLE LOAD

$= \frac{569}{2(\text{SAFETY FACTOR})} \times \frac{1}{46^K} = 6.2$

WHERE 46 IS AXLE LOAD IN KIPS CALCULATED AS FOLLOWS:

264,000# / 4 = 66,000# / AXLE

DUAL WHEEL SPACING ≈ 32" ⇒ EQUIVALENT LOAD FACTOR = 0.7 [REF. 6.6, FIG 18]

$66^K \times 0.7 = 46^K$

REF. 6.6, FIG 16 ⇒ t = 11.2" USING SLAB STRESS OF 6.2 CALCULATED ABOVE. USE t = 12".

EC&FS DEPARTMENT

CALCULATION SHEET

PRELIM. CCN NO. | PAGE ___ OF ___

CCN CONVERSION: CCN NO. CCN -

Project or DCP/FCN _____ Calc No. C-296-01.04

Subject ISFSI FOUNDATION DESIGN Sheet 12 of ___

REV	ORIGINATOR	DATE	IRE	DATE	REV	ORIGINATOR	DATE	IRE	DATE	REV INDICATOR
0	HASSAN HADIDI HH	5/12/01	J. Wang	5/31/01						

CHECK OF AREA REQUIRE FOR THE JACK LOAD

$t^2 = P_u \times A \times \log_{10}\left[\frac{B t^3}{C}\right]$ ← from DESIGNING FLOOR SLABS ON GRADE SECOND EDITION BOYD C. RINGO | ROBERT B. ANDERSON pg 52 [REF. 6.6]

P_u = the factored column load in pounds

$A = 0.03 \times f'c$

$B = 915{,}000 \times \sqrt{f'c}$

$C = K \times b^4$

t = slab thickness

b = base plate dimension, inches

$P_u = 264{,}000 / 4$ (jacks) $= 66{,}000 \times 1.6 = 105{,}600^{\#}$ ← ASSUMED LOAD FACTOR

$A = .03 \times \sqrt{4000} = .000474$

$B = 915{,}000 \times 63.24 = 57{,}869{,}681.$

$C = 200 \times b^4$

$t = 12$

K subgrade modulus Conservative value = 200 pci

$$144 = 105{,}000 \times .000474 \times C = \frac{B t^3}{10\,[t^2/P_u A]} = 200 \times b^4 = \frac{57{,}869{,}681 \times 12^3}{10^{(144/105{,}600 \times .000474)}}$$

(T82)

$b^4 = 639.378$

$b = 28.27''$

$P_u = (12)^2 / \{0.000474 \log_{10}[\frac{57{,}869{,}681/12^3}{200 \times 29^4}]\}$

$= 106{,}619^{\#}$

AREA REQUIRED FOR JACK LOAD $= 29 \times 29 = 841\ in^2$ FOR A $P_u = 105{,}600^{\#}$ LOAD

E&TS DEPARTMENT

CALCULATION SHEET

ICCN NO./ PRELIM. CCN NO.	PAGE ___ OF ___
CCN CONVERSION: CCN NO. CCN -	

Project or DCP/FCN _____ Calc No. C-296-01.04

Subject ISFSI FOUNDATION DESIGN Sheet 13 of ___

REV	ORIGINATOR	DATE	IRE	DATE	REV	ORIGINATOR	DATE	IRE	DATE
0	HASSAN HADIDI HH	3/12/01	J. Wong	5/31/01					

REV INDICATOR

8.0 CALCULATIONS (CONTINUED)

PUNCHING SHEAR CAP = $4\sqrt{f'_c}\, b_o d$ ($b_o = 4(b+d)$; $d = 12'' - 3.25'' = 8.75''$)

$= 4\sqrt{4000}\,(4\times(29''+8.75''))(8.75'')$

$= 334{,}252^{\#} > 105{,}600^{\#}$ O.K.

SLAB DESIGN SUMMARY:

$t = 12''$, #4 @ 12" TOP & BOTTOM, EACH WAY

29"x29" BASE PLATE FOR THE JACK LOAD

Printed on recycled paper

EC&FS DEPARTMENT

CALCULATION SHEET

ICCN NO./ PRELIM. CCN NO. | PAGE ____ OF ____

CCN CONVERSION: CCN NO. CCN -

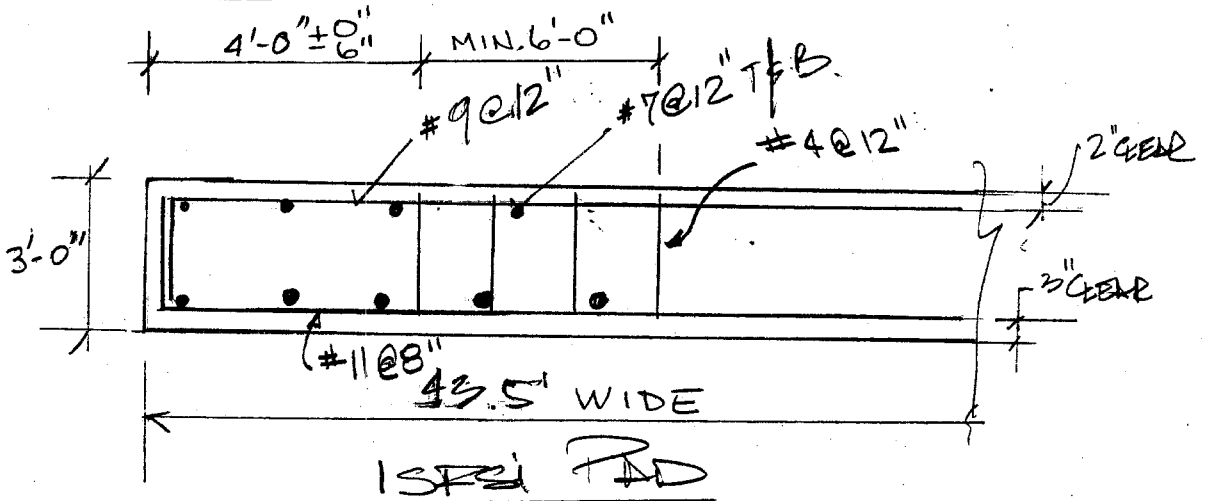
Project or DCP/FCN _____ Calc No. C-296-01.04

Subject ISFSI FOUNDATION DESIGN Sheet 14 of ____

REV	ORIGINATOR	DATE	IRE	DATE	REV	ORIGINATOR	DATE	IRE	DATE
0	HASSAN HADIDI HH	3/12/01	J. Wang	5/31/01					
1	T. Yee S. Yee	4/03/02	JE Appel	4/5/02					

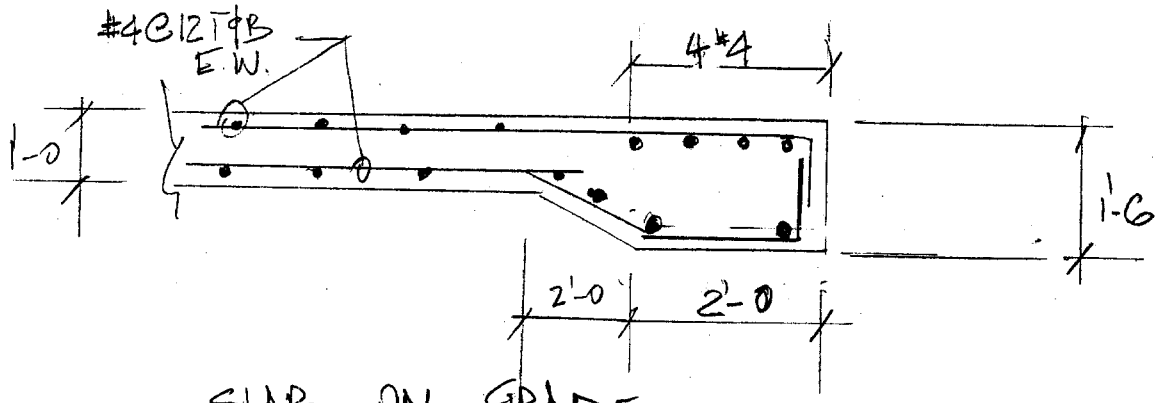
REV INDICATOR

DWG 28002



ISFSI PAD

TYPICAL SECTION



SLAB ON GRADE

E&TS DEPARTMENT

CALCULATION SHEET

ICCN NO./ PRELIM. CCN NO.	PAGE ___ OF ___
CCN CONVERSION: CCN NO. CCN -	

Project or DCP/FCN SONGS 1 Calc No. C-296-01.04

Subject FOUNDATION DESIGN ISFSI Sheet 15 of ___

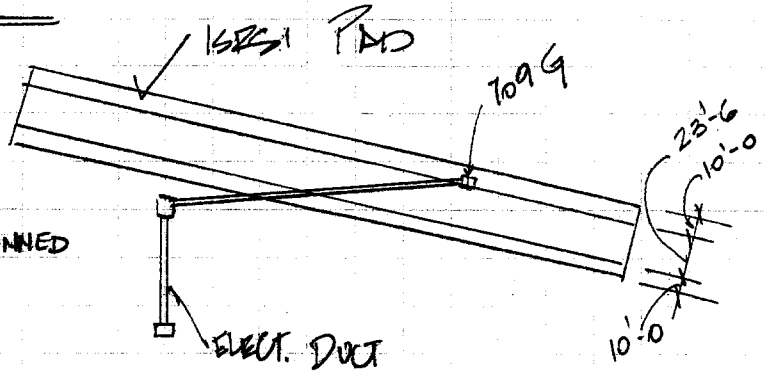
REV	ORIGINATOR	DATE	IRE	DATE	REV	ORIGINATOR	DATE	IRE	DATE
0	HASSAN HADIDI HH	3/12/01	J. Dan	5/21/01					

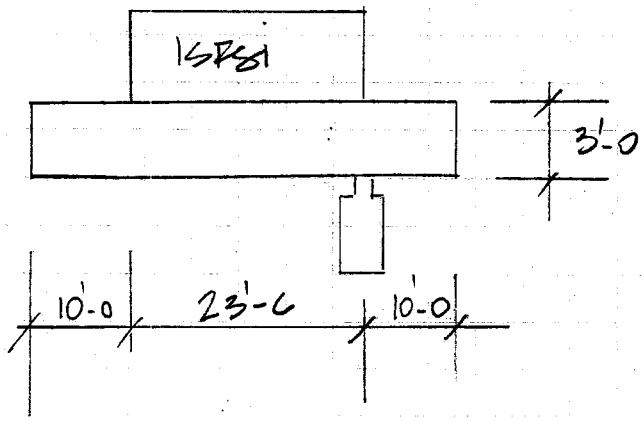
REV INDICATOR

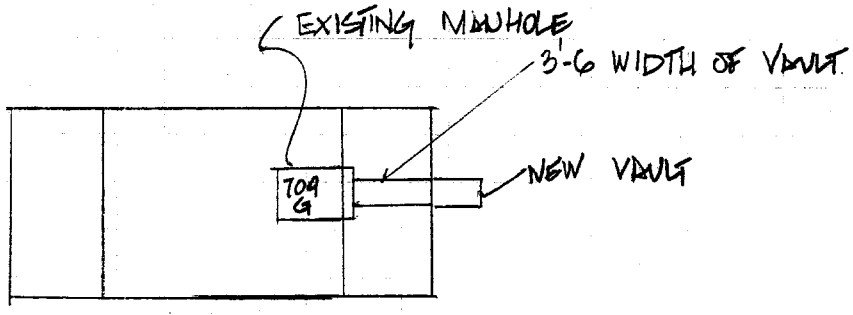
FOUNDATION DESIGN

VAULT DESIGN

VAULT DESIGN IS PROVIDED FOR INFORMATION ONLY. ACCESS TO EXISTING MANHOLE IS NOT PLANNED IN THE CURRENT DESIGN.







AN EXISTING MANHOLE T09G IS LOCATED UNDER ISFSI PAD. FOR INSPECTION OF EXISTING MANHOLE BUILD A VAULT CONNECTING T09G MANHOLE TO THE MANHOLE WHICH WILL BE LOCATED OUTSIDE THE ISFSI PAD. THE SIDE WALLS OF THE VAULT WILL HAVE SAME HEIGHT AS WALLS OF THE EXISTING MANHOLE.

Printed on recycled paper

E&TS DEPARTMENT

CALCULATION SHEET

ICCN NO./ PRELIM. CCN NO.	PAGE ___ OF ___
CCN CONVERSION: CCN NO. CCN -	

Project or DCP/FCN SONGS 1 Calc No. C-296-01.04

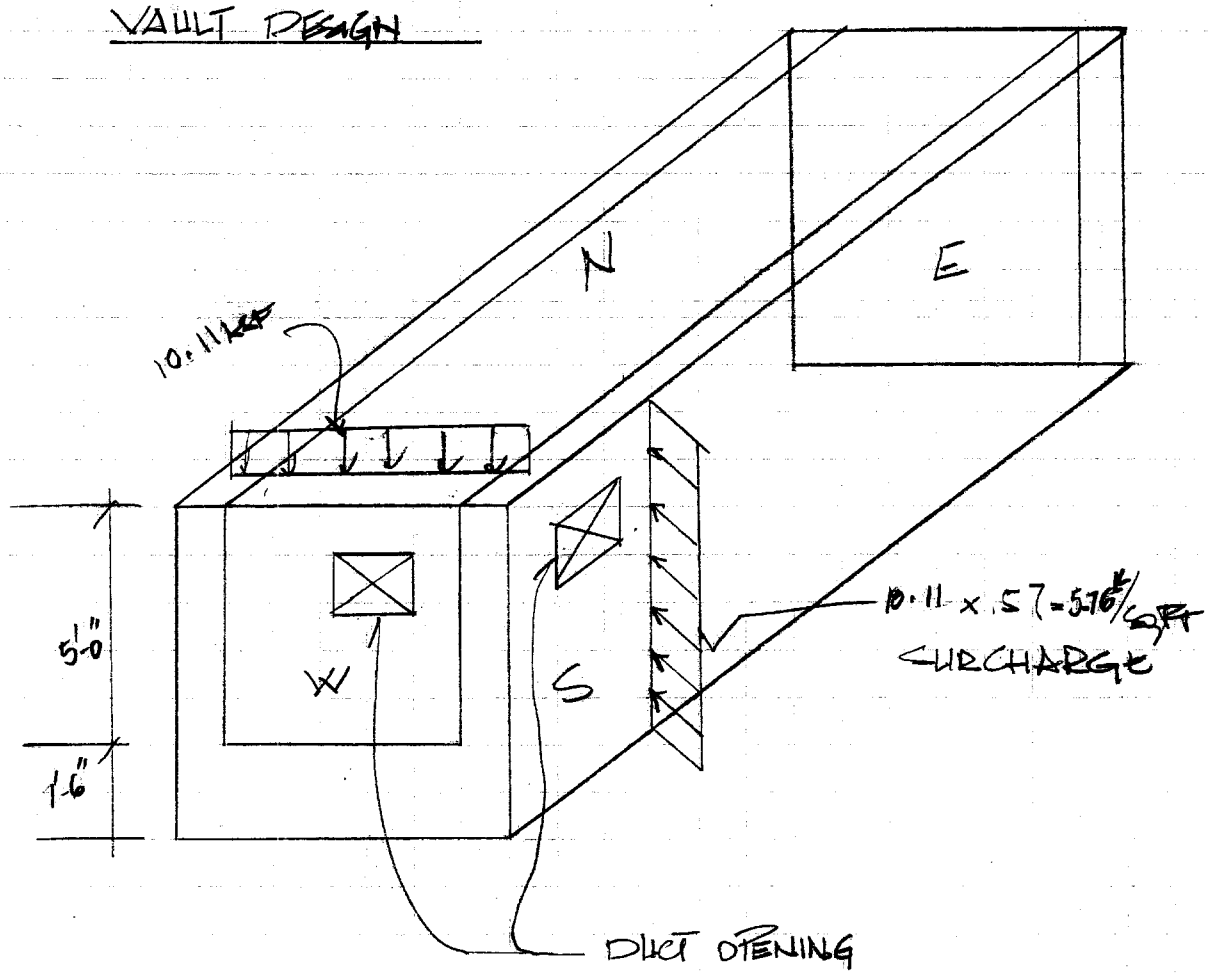
Subject FOUNDATION DESIGN ISFSI Sheet 16 of ___

REV	ORIGINATOR	DATE	IRE	DATE	REV	ORIGINATOR	DATE	IRE	DATE
0	HASSAN HADIDI	3/12/01	J.D.	5/21/01					

REV INDICATOR

FOUNDATION DESIGN ISFSI

VAULT DESIGN



Printed on recycled paper

REV	ORIGINATOR	DATE	IRE	DATE	REV	ORIGINATOR	DATE	IRE	DATE
0	HASSAN HADIDI	3/12/01	J. [illegible]	5/21/01					

REV INDICATOR

8.0 CALCULATIONS (CONTINUED)

WALL DESIGN: CONSIDER TWO LOADING CONDITIONS 1) BEFORE PAD AND MODULES ARE CONSTRUCTED 2) AFTER PAD AND MODULES ARE CONSTRUCTED.

1) BEFORE PAD CONSTRUCTION, CANTILEVER WALL, TENSION REBAR OUTSIDE FACE, MAX. MOMENT AT THE BASE OF THE WALL:

D+L LOADS:

$M_1 = \frac{1}{6}(K_a \gamma) h^3$ DUE TO SOIL

$M_1 = \frac{1}{6}(0.57 \times 0.126)(5)^3 = 1.50$ K-FT/FT

$M_2 = \frac{w l^2}{2} = (0.45 \times 0.57)(5)^2/2 = 3.21$ K-FT/FT (PAD WT, K_a)

ADD THIS TO ACCOUNT FOR THE SURCHARGE LOADING DUE TO PAD WEIGHT BEFORE THE CONNECTION BETWEEN PAD AND WALL IS 100% EFFECTIVE.

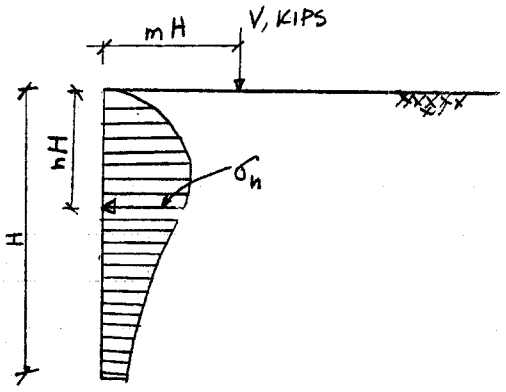
M_3 = MOMENT DUE TO SURCHARGE FROM THE WHEEL LOADS (REF. 6.9, PAGE 415)

Printed on recycled paper

REV	ORIGINATOR	DATE	IRE	DATE	REV	ORIGINATOR	DATE	IRE	DATE
0	HASSAN HADIDI	5/7/01	[signature]	5/21/01					

REV INDICATOR

8.0 CALCULATIONS (CONTINUED)



$m > 0.4 \quad \sigma_h = \frac{1.77V}{H^2} \frac{m^2 n^2}{(m^2+n^2)^3}$

$m \leq 0.4 \quad \sigma_h = \frac{0.28V}{H^2} \frac{n^2}{(0.16+n^2)^3}$

FOR A GIVEN V, $m = 0.4 \Rightarrow$ MAXIMUM σ_h

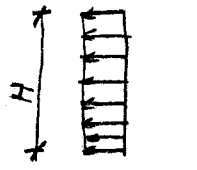
∴ USE $\sigma_h = \frac{0.28V}{H^2} \frac{n^2}{(0.16+n^2)^3}$

$V = 16^K$ (WHEEL LOAD)

$H = 5'$

n	σ_h (KSF)	
0	0	
0.1	0.36	
0.2	0.90	
0.25	1.02	
0.26	1.02	
0.27	1.03	
0.28	1.04	← MAXIMUM
0.29	1.04	
0.3	1.03	
0.35	0.97	
0.4	0.88	
0.5	0.65	
0.6	0.46	
0.7	0.32	
0.8	0.22	
0.9	0.16	
1.0	0.11	

CONSERVATIVE USE $\sigma_h = 1.04$ KSF UNIFORMLY OVER FULL HEIGHT.



$M_3 = 1.04\,(5')(5'/2)$

$M_3 = 13$ K-FT/FT

Printed on recycled paper

REV	ORIGINATOR	DATE	IRE	DATE	REV	ORIGINATOR	DATE	IRE	DATE
0	HASSAN HADIDI HH	5/7/01	J. Wang	5/21/01					

REV INDICATOR

8.0 CALCULATIONS (CONTINUED)

LOAD FACTOR DUE TO EARTH PRESSURE ← $1.7 M_1$ + $1.4 M_2$ + $1.7 M_3$ → L.L.
D.L.

$M_u = 1.7(1.50) + 1.4(3.21) + 1.7(13) = 29.1$ K-FT/FT

2) AFTER PAD AND MODULE ADDED:

SEISMIC LOAD CASE:

$$M = \frac{w h^2}{8} + \frac{1}{2}\left[\frac{1}{6}(K_a \gamma) h^3\right]$$ MAXIMUM @ WALL MID HEIGHT

$$M = \frac{(0.57 \times 10.11)(5)^2}{8} + \frac{1}{2}\left[\frac{1}{6}(0.57 \times 0.126)(5)^3\right] = 18.8 \text{ K-FT/FT}$$

∴ DESIGN WALLS FOR 29.1 K-FT/FT

Printed on recycled paper

E&TS DEPARTMENT

CALCULATION SHEET

ICCN NO./ PRELIM. CCN NO.	PAGE ___ OF ___
CCN CONVERSION: CCN NO. CCN -	

Project or DCP/FCN _____ Calc No. C-296-01.04

Subject ISFSI FOUNDATION DESIGN Sheet 20 of ___

REV	ORIGINATOR	DATE	IRE	DATE	REV	ORIGINATOR	DATE	IRE	DATE
0	HASSAN HADID HH	3/12/01	J. Wang	5/21/01					

REV INDICATOR

8.0 CALCULATIONS (CONTINUED)

$$\rho_s = \frac{0.85 f'c}{fy}\left[1 - \sqrt{1 - \frac{2K_u}{\phi(.85)(f'c)}}\right]$$

$$K_u = \frac{M \times 12000}{bd^2} = \frac{29.1 \times 12000}{12 \times 15^2} = 129.3$$

$$\rho_s = \frac{0.85 \times 4}{60}\left[1 - \sqrt{1 - \frac{2 \times 129.3}{0.9 \times 0.85 \times 4000}}\right] = 0.0024$$

USE $\rho_{MIN} = 0.0033$ FOR VERTICAL REBARS $\approx \frac{4}{3}\rho_s = 0.0032$ O.K.

$A_s = 0.0033 \times 12 \times 15 = 0.59$ IN²/FT

USE #8 @ 12" USE SAME REINFORCING FOR INSIDE AND OUTSIDE FACES
0.79 IN²/FT > 0.59 IN²/FT O.K.

$\phi M_n = 0.9 \times 0.79 \times 60\left[15 - \frac{1}{2}\frac{0.79 \times 60}{.85 \times 4 \times 12}\right]/12 = 51.3$ K-FT/FT > 29.1 K-FT/FT O.K.

HORIZONTAL REINF: $0.0025 \times 12 \times 15/2 = 0.23$ IN²/FT/FACE
≤ ρ_{MIN}

USE #6 @ 12" EACH FACE = 0.44 IN²/FT/FACE > 0.23 O.K.

∴ VERTICAL #8 @ 12" EACH FACE

HORIZONTAL #6 @ 12" EACH FACE

Printed on recycled paper

E&TS DEPARTMENT

CALCULATION SHEET

ICCN NO./ PRELIM. CCN NO.	PAGE ___ OF ___
CCN CONVERSION: CCN NO. CCN -	

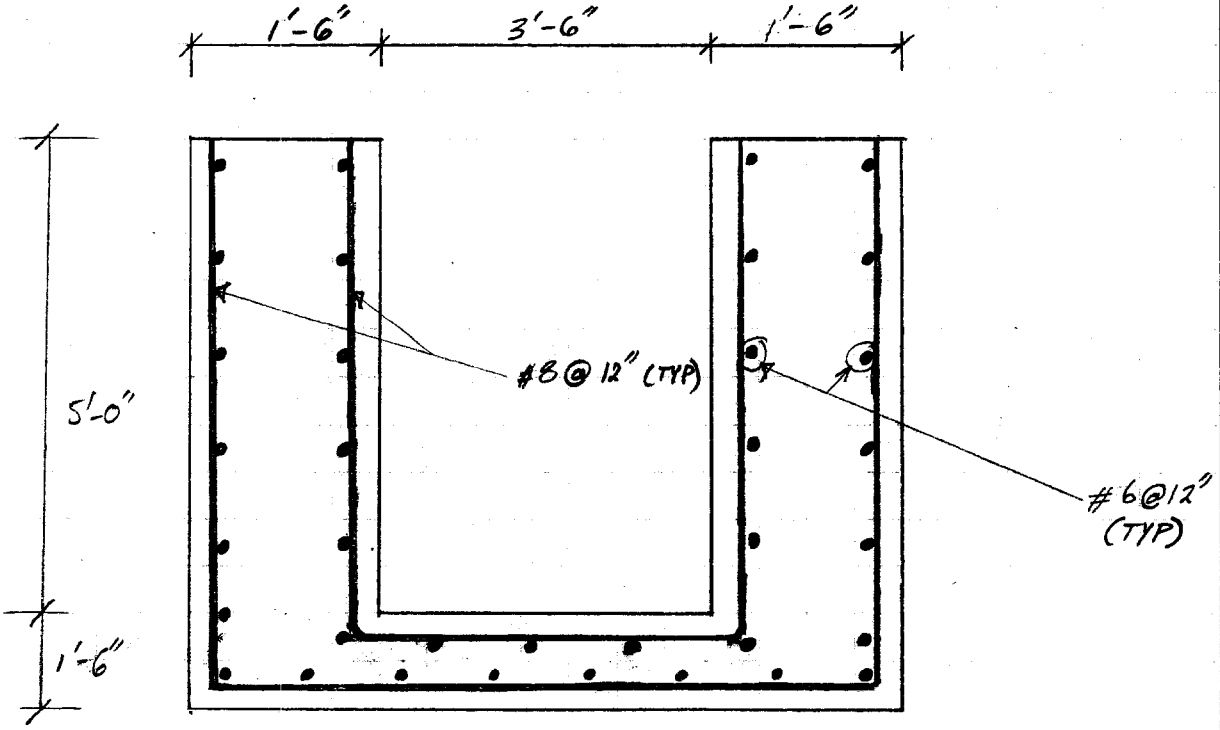
Project or DCP/FCN _____ Calc No. C-296-01-04

Subject ISFSI FOUNDATION DESIGN Sheet 21 of ___

REV	ORIGINATOR	DATE	IRE	DATE	REV	ORIGINATOR	DATE	IRE	DATE
0	HASSAN HADIDI	3/12/01	J.W. Dong	5/2/01					

REV INDICATOR

8.0 CALCULATIONS (CONTINUED)



Printed on recycled paper

EC&FS DEPARTMENT

CALCULATION SHEET

ICCN NO./ PRELIM. CCN NO.	PAGE ____ OF ____
CCN CONVERSION: CCN NO. CCN -	

Project or DCP/FCN _____ Calc No. C-296-01.04

Subject ISFSI FOUNDATION DESIGN Sheet 7N of ____

REV	ORIGINATOR:	DATE	IRE	DATE	REV	ORIGINATOR	DATE	IRE	DATE	REV INDICATOR
0	HASSAN HADIDI HH	12/26/00	J. Wong	5/21/01						

CHECK BOTTOM SLAB

TOP SLAB D.L. $150 \times (3.5+1.5+1.5) \times 1.4 \times 3 \times 1 = 4,095$ LB/FT

BOTTOM SLAB D.L. $150 \times (3.5+1.5+1.5) \times 1.4 \times 1.5 \times 1 = 2,048$ LB/FT

SIDE WALLS D.L. $150 \times 5 \times 1.5 \times 2 \times 1.4 \times 1 = 3,150$ LB/FT

LIVE LOAD $100 \times 3.5 \times 1 \times 1.7 = 595$ LB/FT

D.L. FROM PAD $[(471^K + 166^K)/(43.5' \times 8.5')] \times 1.4 \times (3.5'+1.5'+1.5') = 15,677$ LB/FT

25,565 LB/FT

(471K: MODULE WT; 166K: WT OF PAD)

BOTTOM SOIL PRESSURE = (25,565 LB/FT) / (3.5'+1.5'+1.5') = 3,933 PSF

$V_u = 3,933 \text{ PSF} \times 3.5' / 2 = 6,883^{\#}/\text{FT}$

$\phi V_c = 0.85 \times 2\sqrt{4,000} \times 12'' \times 15'' = 19,353^{\#}/\text{FT} > 6,883^{\#}/\text{FT}$ O.K.

$M_u = 3,933 (3.5')^2/8 = 602$ K-FT/FT

$K_u = M_u/bd^2 = 602 \times 12000/[(12)(15)^2] = 26.8$

$\rho = \frac{0.85f'_c}{f_y}\left[1 - \sqrt{1 - \frac{2K_u}{\phi(.85)f'_c}}\right] = \frac{0.85 \times 4}{60}\left[1 - \sqrt{1 - \frac{2 \times 26.8}{.9 \times .85 \times 4,000}}\right]$

$\rho = 0.00050 < \rho_{MIN}$

$\rho_{MIN} = 200/f_y = 200/60,000 = 0.0033$ USE $\rho = \rho_{MIN} = 0.0033$

EC&FS DEPARTMENT

CALCULATION SHEET

ICCN NO./ PRELIM. CCN NO.	PAGE ____ OF ____
CCN CONVERSION: CCN NO. CCN -	

Project or DCP/FCN _____ Calc No. C-296-01.04

Subject ISFSI FOUNDATION DESIGN Sheet 27 of ____

REV	ORIGINATOR:	DATE	IRE	DATE	REV	ORIGINATOR	DATE	IRE	DATE	REV INDICATOR
0	HASSAN HADIDI HA	12/26/00	J. Wang	5/21/01						

USE #8 @ 12" TO MATCH THE WALL REINFORCING

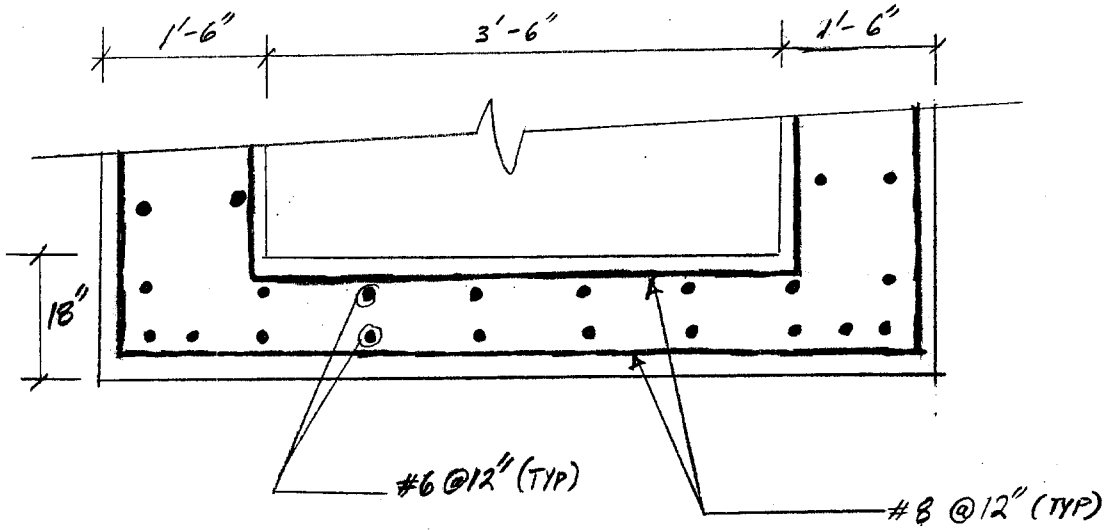
$$\rho = \frac{0.79\,IN^2}{(12")(15")} = 0.0044 > 0.0033 \quad O.K.$$

$$\phi M_n = 0.9 \times 0.79 \times 60 \left[15 - \frac{1}{2}\,\frac{0.79 \times 60}{0.85 \times 4 \times 12}\right] / 12 = 51.3\ K\text{-}FT/FT > 6.02\ K\text{-}FT/FT\ O.K.$$

USE #6 @ 12" LONGITUDINAL REINFORCING (SAME AS WALL HORIZONTAL REINFORCING)

$$\rho = \frac{0.44\,IN^2 \times 2}{12" \times 18"} = 0.0041 > 0.0018\ MIN.\ SHRINKAGE\ REINF\ O.K.$$

(2 ← TOP & BOTTOM; 12" × 18" ← ON CROSS CONC. AREA)



E&TS DEPARTMENT

CALCULATION SHEET

ICCN NO./ PRELIM. CCN NO.	PAGE ___ OF ___
CCN CONVERSION: CCN NO. CCN -	

Project or DCP/FCN _____ Calc No. C-296-1.04

Subject ISFSI FOUNDATION DESIGN Sheet 24 of ___

REV	ORIGINATOR	DATE	IRE	DATE	REV	ORIGINATOR	DATE	IRE	DATE	REV INDICATOR
0	HASSAN HADIDI	3/12/01	J. Wang	5/21/01						

8.0 CALCULATIONS (CONTINUED)

DESIGN THE STEEL PLATE TO COVER THE EXISTING MANHOLE: (DWG. 28010).

DESIGN LOAD: H20 TRUCK LOAD OF 32^K PER AXLE, 16^K EACH SET OF WHEELS, 6' APART. ADD THE DEAD LOAD DUE TO 3' OF SOIL COVERING THE STEEL PLATE.

γ_{SOIL} ← HALF OF DISTANCE BETWEEN WHEELS

$$M = \frac{16^K(6')}{4}(1.3) + \frac{(3' \times 0.126 \times 3')(6')^2}{8}$$

(1.3) ← IMPACT FACTOR (REF. 6.10 PAGE 18-17)

$= 31.2$ K-FT $+ 5.1$ K-FT $= 36.3$ K-FT

$$\text{PLATE THICKNESS} = t = \sqrt{\frac{(36.3 \text{ K-FT})(12)}{\underbrace{(0.75 \times 36 \text{ KSI})}_{f_b = 0.75 f_y}\ (3' \times 12'')/6}}$$

$(3' \times 12'')/6$ ← HALF OF DISTANCE BETWEEN WHEELS

$t = 1.64''$ USE $1\frac{3}{4}''$ PLATE

$$\text{MOMENT CAPACITY} = f_b S = (0.75 \times 36 \text{ KSI})(36'' \times 1.75^2/6)/12 = 41.3 \text{ K-FT}$$

> 36.3 K-FT O.K.

IMPACT LOAD FACTOR; γ_{SOIL}; HALF OF DIST. BETWEEN WHEELS

$$\Delta = \frac{16^K(1.3)(72)^3}{48 \times 29{,}000 \times 16.1} + \frac{5[(3' \times 0.126 \times 3')/12](72)^4}{384 \times 29{,}000 \times 16.1} = 0.35'' + 0.07'' = 0.42''$$

O.K.

$I = \frac{1}{12}(36'')(1.75)^3 = 16.1 \text{ IN}^4$

HALF OF DISTANCE BETWEEN WHEELS

Printed on recycled paper

E&TS DEPARTMENT

CALCULATION SHEET

ICCN NO./ PRELIM. CCN NO.	PAGE ___ OF ___
CCN CONVERSION: CCN NO. CCN -	

Project or DCP/FCN _____ Calc No. C-296-1.04

Subject 15FS1 FOUNDATION DESIGN Sheet 25 of ____

REV	ORIGINATOR	DATE	IRE	DATE	REV	ORIGINATOR	DATE	IRE	DATE	REV INDICATOR
0	HASSAN HADIDI	3/12/01	J. Wang	5/21/01						

8.0 CALCULATIONS (CONTINUED)

DESIGN THE STEEL PLATE TO COVER THE VAULT :

$$M = \frac{16^{K}(3.5')}{4}(1.3) + \frac{(3'\times 0.126\times 3')(3.5')^2}{8}$$

$$= 18.2\ K\text{-}FT + 1.7\ K\text{-}FT = 19.9\ K\text{-}FT$$

$$\text{PLATE THICKNESS} = t = \sqrt{\frac{(19.9\ K\text{-}FT)(12)}{(0.75\times 36\ KSI)(3'\times 12'')/6}}$$

$$t = 1.21 \qquad \text{USE } 1\tfrac{1}{4}'' \text{ PLATE}$$

$$\text{MOMENT CAPACITY} = f_b S = (.75\times 36\ KSI)(36\times 1.25^2/6)/12 = 21.1\ K\text{-}FT$$

$$> 19.9\ K\text{-}FT$$

O.K.

$$\Delta = \frac{16^{K}(1.3)(42)^3}{48\times 29{,}000\times 5.9} + \frac{5\left[(3'\times 0.126\times 3')/12\right](42)^4}{384\times 29{,}000\times 5.9}$$

$I = \frac{1}{12}(36'')(1.25)^3 = 5.9$

$$\Delta = 0.19'' + 0.02'' = 0.21'' \quad \text{O.K.}$$

Printed on recycled paper

E&TS DEPARTMENT

CALCULATION SHEET

ICCN NO./ PRELIM. CCN NO.	PAGE ___ OF ___
CCN CONVERSION: CCN NO. CCN -	

Project or DCP/FCN _____ Calc No. C-296-01.04

Subject ISFSI FOUNDATION DESIGN Sheet 26 of 28

REV	ORIGINATOR	DATE	IRE	DATE	REV	ORIGINATOR	DATE	IRE	DATE	REV INDICATOR
0	HASSAN HADIDI	5/11/01	J. Wang	5/11/01						

8.0 CALCULATIONS (CONTINUED)

CHECK EXISTING MANHOLE FOR THE PAD PLUS SEISMIC LOADS:

SINCE CONCRETE HAS A HIGHER STIFFNESS THAN THE SURROUNDING SOILS, THE PAD AND MODULE SEISMIC LOADS WILL BE MOSTLY RESISTED BY THE MANHOLE WALLS IN BEARING.

CHECK THE BEARING STRESS ON THE EXISTING MANHOLE WALLS:

TOTAL BEARING LOAD = $(10.11 \text{ KSF})(7.67' \times 7.67') = 595^{K}$

$\phi P_n = 0.7 P_n = 0.7 \times 0.85 f'_c \times A_c = 0.595 f'_c A_c$

$A_c = (4 \times 82'' - 42)(10'') = 2860 \text{ IN}^2$

↑ 3'-6 OF MANHOLE WALL TO BE REMOVED

$\phi P_n = 0.595 \times 4 \times 2860 = 6807^{K} > P_u = 595^{K}$ O.K.

↑ ASSUME $f'_c = 4000$ PSI

Printed on recycled paper

EC&FS DEPARTMENT

CALCULATION SHEET

ICCN NO./ PRELIM. CCN NO.	PAGE ___ OF ___
CCN CONVERSION: CCN NO. CCN -	

Project or DCP/FCN SONGS 1 Calc No. C-296-01.04

Subject ISFSI Foundation Design Sheet 27 of ___

REV	ORIGINATOR	DATE	IRE	DATE	REV	ORIGINATOR	DATE	IRE	DATE	REV INDICATOR
2	T. Yee	3/4/03		3/24/03						

CHECK CONCRETE PAD TARGET HARDNESS

Per Section 12.4.4.2 of TN SAR (Ref. 6.4), the concrete pad properties must meet the concrete parameters specified in EPRI Report NP-4830, "The Effects of Target Hardness on the Structural Design of Concrete Storage Pads for Spent Fuel Casks," October 1986. In order to meet this requirement, the target hardness will be calculated and must be less than 400,000. TN West drop analysis used a max. acceleration of 75g which corresponds to a target hardness of 400,000 (EPRI Report, Fig. 28).

The target hardness equations are given the EPRI Report (Equations 4 and 5) as:

$S = 2r - A k M_u \sigma_u / (W^3 (1 - e^{-\beta r} \cos \beta r))$ End Drop

$S = 2 A E_s M_u \sigma_u / (W^3 \beta)$ Edge Drop

NOTE: Edge Drop is the same as Side Drop for TN analysis.

Printed on recycled paper

REV	ORIGINATOR	DATE	IRE	DATE	REV	ORIGINATOR	DATE	IRE	DATE
2	T. Yee	3/4/03		3/24/03					

REV INDICATOR

CHECK CONCRETE PAD TARGET HARDNESS (CONT.)

where:

S = target hardness number (non dimensional)

M_u = ultimate moment capacity of the slab (lb-in)

W = weight of Cask (lb.)

σ_u = ultimate strength of concrete (psi)

A = cask footprint area (in^2)

E_s = elastic modulus of soil

E_c = elastic modulus of concrete

ν_s = Poisson's ratio of soil

ν_c = Poisson's ratio of concrete = .17 (EPRI Report)

r = cask radius

End Drop

$$\beta = (E_s / 4D_c)^{1/4}$$

$$D_c = E_c h^3 / (12(1-\nu_c^2))$$

$$k = \pi E_s / (1-\nu_s^2)$$

Printed on recycled paper

CHECK CONCRETE PAD TARGET HARDNESS (CONT.)

h = concrete pad thickness

Edge Drop

$$\beta = (E_s/4E_cI_c)^{1/4}$$

$$I_c = \frac{1}{12} L h^3$$

L = length of cask = 203 in. (Ref. SO1-207-1-D173)

Target Hardness - End Drop:

$$r = \frac{80}{2} = 40"$$ (Ref. SO1-207-1-D173)

$$A = \pi r^2 = \pi (40)^2$$
$$= 5026\ in^2$$

E_s = 13000 ksf (Ref. SONGS 2&3 FSAR, Sect. 2.5.4.10.4)
= 90,278 psi

ν_s = .35

$$k = \pi E_s/(1-\nu_s^2) = \pi (90278)/(1-.35^2)$$
$$= 323,210$$

$$M_u = \frac{M_{CAP}}{.9} = \frac{322}{.9} = 358\ k\text{-}ft = 4.293 \times 10^6\ lb\text{-}in$$

σ_u = 4000 psi

W = 200,000 lb. (Ref. SO1-207-1-C11)

Printed on recycled paper

REV	ORIGINATOR	DATE	IRE	DATE	REV	ORIGINATOR	DATE	IRE	DATE
2	T. Yee TY	3/4/03	[illegible]	3/24/03					

REV INDICATOR

CHECK CONCRETE PAD TARGET HARDNESS (CONT.)

$$D_c = E_c h^3 / (12(1-\nu_c^2))$$

$$= \frac{3.6\times10^6 (36)^3}{12(1-.17^2)}$$

$$= 1.44\times10^{10}$$

$$E_c = 57000\sqrt{f'_c}$$
$$= 57000\sqrt{4000}$$
$$= 3.6\times10^6 \text{ psi}$$

$$\beta = \left(\frac{E_s}{4D_c}\right)^{\frac{1}{4}} = \left[\frac{90278}{4(1.44\times10^{10})}\right]^{\frac{1}{4}}$$

$$= .0354$$

$$S = \frac{2(40)(5026)(323210)(4.293\times10^6)(4000)}{200000^3\left(1-e^{-.0354(40)}\cos .0354(40)\right)}$$

$$= 368{,}305 \quad (\text{End Drop}) \quad < 400{,}000 \quad \underline{\text{OK}}$$

Target Hardness – Edge Drop (Side Drop):

$$A = DL = 10\times203$$
$$= 2030 \text{ in}^2$$

$$I_c = \frac{1}{12}Lh^3 = \frac{1}{12}(203)(36)^3$$
$$= 789{,}264 \text{ in}^4$$

$$\beta = \left(\frac{E_s}{4E_cI_c}\right)^{\frac{1}{4}} = \left(\frac{90278}{4(3.6\times10^6)(789264)}\right)^{\frac{1}{4}}$$

$$= .0094$$

Printed on recycled paper

REV	ORIGINATOR	DATE	IRE	DATE	REV	ORIGINATOR	DATE	IRE	DATE	REV INDICATOR
2	T. Yee	3/4/03		3/24/03						

CHECK CONCRETE PAD TARGET HARDNESS (CONT.)

$$S = \frac{2(2030)(90278)(4.293\times10^{6})(4000)}{200000^{3}(.0094)}$$

$= 83{,}697 < 400{,}000$ OK.
(Edge Drop or Side Drop)

∴ The concrete pad and soil at SONGS have target hardnesses of less than 400,000. Therefore, the TN West cask drop analysis is valid for SONGS.

Although the end drop case was evaluated on ISFSI pad, the scenario is not credible because the transfer cask cannot fall on its end from the transfer trailer. Also, there is sufficient margin to account for actual concrete strength for the edge drop case (Target Hardness is proportional to concrete strength)

Printed on recycled paper

E&TS DEPARTMENT

CALCULATION SHEET

ICCN NO./ PRELIM. CCN NO.	PAGE ____ OF ____
CCN CONVERSION: CCN NO. CCN -	

Project or DCP/FCN SONGS 1 Calc No. C-296-01.04

Subject ISFSI Foundation Design Sheet 32 of ___

REV	ORIGINATOR	DATE	IRE	DATE	REV	ORIGINATOR	DATE	IRE	DATE	REV INDICATOR
2	T. Yee TY	3/4/03	J. Appel	3/24/03						↓

Pad Inspection

The concrete pad was inspected for cracks and the results of the inspection are noted on the following sheet which indicates the approximate crack widths and the locations of the cracks.

The concrete pad was inspected on 7/24/2002 before the Large Component Removal (LCR) crane was placed on the pad. At that time only Cracks A, B and C were noted because they were about 0.1 mm or larger.

A subsequent inspection was performed on 12/3/2002 after the LCR crane was demobilized to see if the condition of the concrete pad had changed significantly. More cracks were observed and the transverse pattern of the cracks is indicative of cracks caused by concrete shrinkage. The cracks were less than 0.4 mm wide and thus classified as "hairline" with the exception of Crack C. Some portions of Crack C were about 0.5 mm wide which is classified as "fine," but there were no other signs of distress. All the cracks are acceptable per the acceptance criteria for concrete cracks that are given in Calc. No. S-02-C-001.

Some edge spalls were also observed and the movement of the crane's crawler tracks over the pad caused these cracks. No rebar was exposed and these spalls were repaired to ensure proper concrete cover over the rebars.

Conclusion:

The concrete condition of the pad is acceptable for the storage modules and the noted results of the inspection will be the baseline for future inspections.

EC&FS DEPARTMENT

CALCULATION SHEET

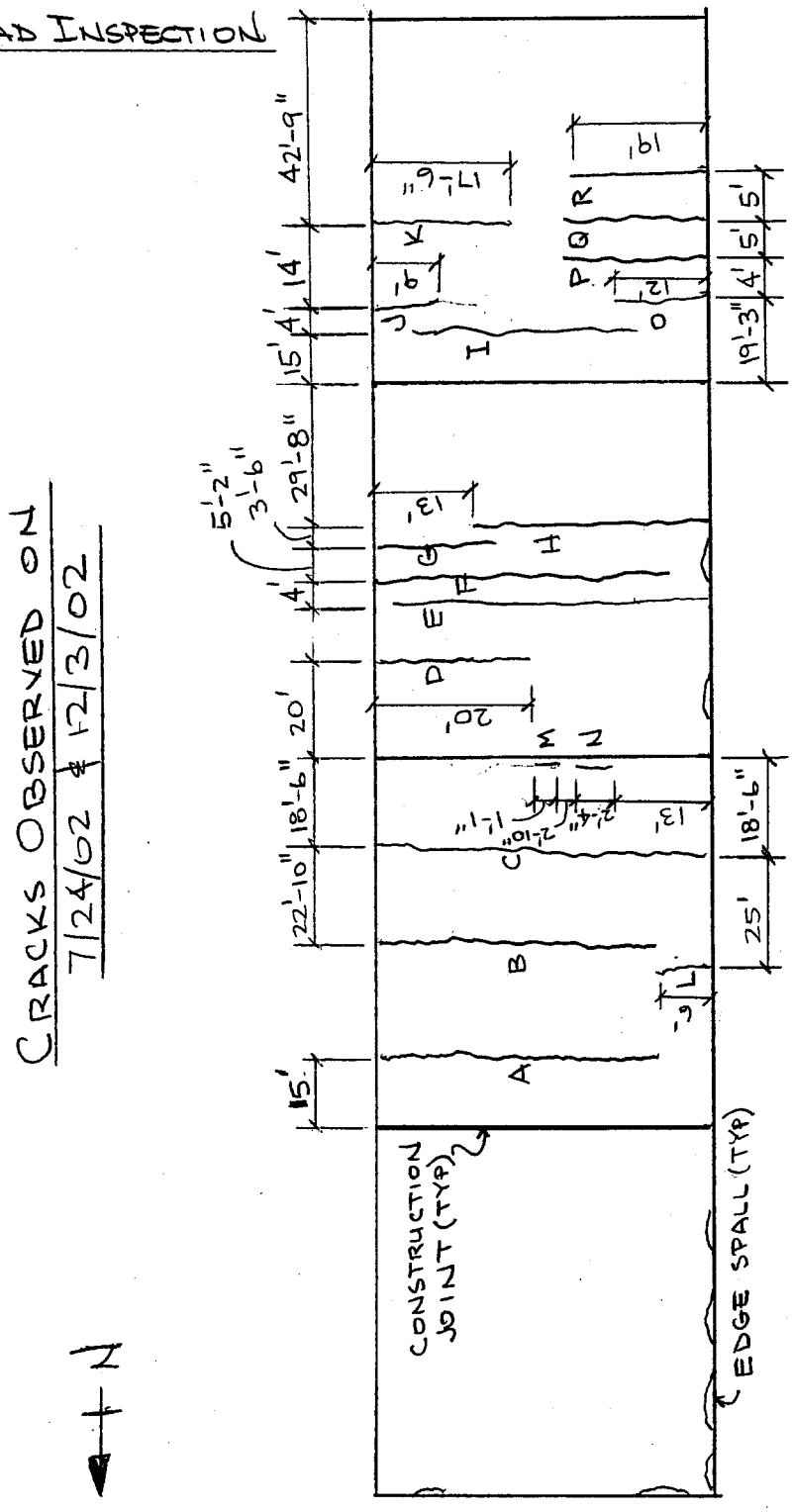
ICCN NO./ PRELIM. CCN NO.	PAGE ___ OF ___
CCN CONVERSION: CCN NO. CCN -	

Project or DCP/FCN SONGS 1 Calc No. C-296-01.04

Subject ISFSI FOUNDATION DESIGN Sheet 33 of 37 (2)

REV	ORIGINATOR	DATE	IRE	DATE	REV	ORIGINATOR	DATE	IRE	DATE	REV INDICATOR
2	T. Yee SY	3/4/03	JE	3/24/03						
3	Luan Pham	5/16/07	T. Yee	8/3/07						

PAD INSPECTION



CRACKS OBSERVED ON 7/24/02 & 12/3/02

PLAN

CRACKS	WIDTH (7/24/02)	WIDTH (12/3/02)
A	.1mm	.1mm
B	.2mm	.3mm
C	.3mm	.4 to .5mm
D	—	.2mm
E	—	.1mm
F	—	.4mm
G	—	.1mm
H	—	.2mm
I	—	.2mm

CRACKS	WIDTH (12/3/02)
J	.1mm
K	.2mm
L	.2mm
M (Edge Crack)	.1mm
N (Edge Crack)	.2mm
O	.1mm
P	.1mm
Q	.1mm
R	.1mm

Printed on recycled paper

E&TS DEPARTMENT

CALCULATION SHEET

ECN NO./ ~~A48347~~ 4 5/16/07 PRELIM. CCN NO.	PAGE ____ OF ____
	CCN CONVERSION: CCN NO. CCN -

Project or ECP 061000254-2 Calc No. C-296-01.04

Subject ISFSI FOUNDATION DESIGN Sheet 34 of ____

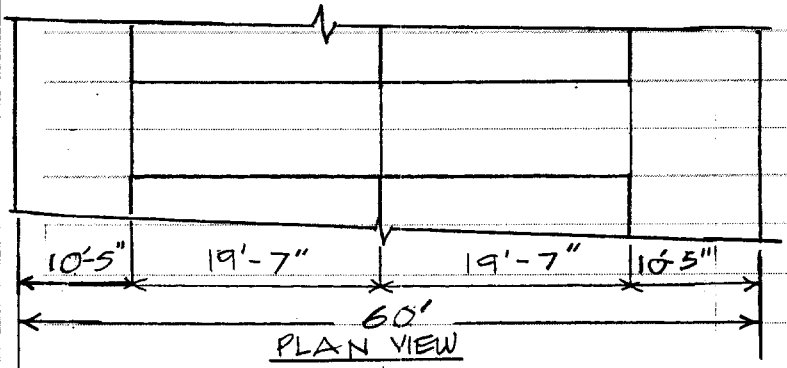
REV	ORIGINATOR	DATE	IRE	DATE	REV	ORIGINATOR	DATE	IRE	DATE	REV INDICATOR
3	L. Pham	2/26/2007	T. Yee	8/3/07						

ISFSI FOUNDATION FOR BACK TO BACK MODULES

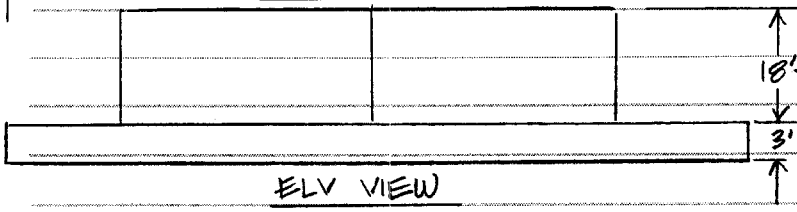
DIMENSIONS: 293'L x 60'W x 3'D [REF: 28002, ECN A46647]

BACK TO BACK MODULES PIMENSIONS:

39'-2"L x 8'-5"W x 18'-6"H [REF: SO1-207-1. M135]



PLAN VIEW



ELV VIEW

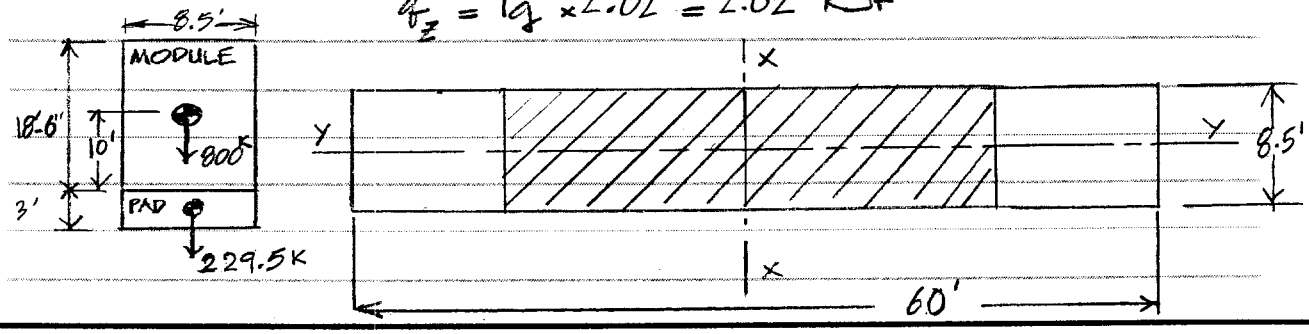
- MODULES WEIGHT: 400 x 2 = 800 KIPS
  (NO REAR SHIELD WALL FOR BACK TO BACK MODULES).
- FOUNDATION WEIGHT 60 x 3 x 8.5 x 0.15 = 229.5 KIPS. [8.5' STRIP]

TOTAL WEIGHT 800 + 229.5 = 1029.5, SAY 1030KIPS

CHECK SOIL PRESSURE:

SOIL PRESSURE DUE TO DEAD LOAD: $q_{PL} = \frac{V}{A} = \frac{1030}{8.5 \times 60} = 2.02$ KSF

SEISMIC VERTICAL: $q_z = 1g \times 2.02' = 2.02'$ KSF



E&TS DEPARTMENT

CALCULATION SHEET

ECN NO./ ~~A48347~~ 4/5/16/07 PRELIM. CCN NO.	PAGE ____ OF ____
	CCN CONVERSION: CCN NO. CCN -

Project or ECP 061000254-2 Calc No. C-296-01.04

Subject ISFSI FOUNDATION DESIGN Sheet 35 of ____

REV	ORIGINATOR	DATE	IRE	DATE	REV	ORIGINATOR	DATE	IRE	DATE
3	L. Pham	2/26/2007	T. Yee	8/3/07					

REV INDICATOR

SEISMIC SOIL PRESSURE ABOUT X-X:

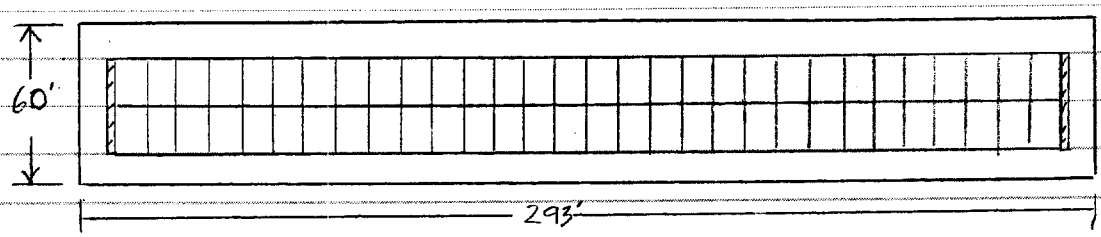
USE ACCELERATION OF 1.0 g FOR BOTH LATERAL & LONGITUDINAL DIR.

$$OTM_x = 1.0g(800\times13)+1.5g(230\times1.5) = 10918 \text{ K-FT}$$

$$e_x = \frac{OTM_x}{V} = \frac{10918}{1030} = 10.6 \text{ FT} > \frac{L}{6} = \frac{60}{6} = 10 \text{ FT}$$

$$q_{fx} = \frac{2V}{3B\left(\frac{L}{2}-e\right)} = \frac{2\times1030}{3(8.5)\left(\frac{60}{2}-10.6\right)} = 4.164 \text{ KSF}$$

SEISMIC SOIL PRESSURE ABOUT Y-Y



FOUNDATION WEIGHT. $60'\times293'\times3\times0.15 = 7911$ K

MODULES' WEIGHT $31\times800 = 24800$ K

END SHIELD WALLS: $(39.17\times18.5\times3\times0.15)2 = 652$ K

TOT = 33363 K

$$OTM_y = 1.0g(24800+652)(13)+1.5g(7911\times1.5) = 330,876+17800$$
$$= 348,676 \text{ FT-K}$$

$$e_y = \frac{M}{V} = \frac{348,676}{33,363} = 10.45 < \frac{L}{6} = \frac{293}{6} = 48.83 \text{ FT}$$

$$q_{fy} = \frac{MC}{I} \quad \text{WHERE} \quad C = \frac{293}{2}, \quad I = \frac{60(293)^3}{12} = 1.26\times10^8 \text{ FT}^4$$

$$q_{fy} = 0.41 \text{ KSF}$$

$$q_{TOT} = q_n + \left[q_x^2 + q_y^2 + q_z\right]^{1/2} = 2.02 + \left[4.164^2 + 0.41^2 + 2.02^2\right]^{1/2} = 6.67 \text{ KSI}$$

E&TS DEPARTMENT

CALCULATION SHEET

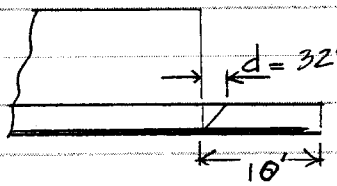
ECN NO./ ~~A48347~~ 4p 5/16/07 PRELIM. CCN NO.	PAGE ____ OF ____
CCN CONVERSION: CCN NO. CCN -	

Project or ECP 061000254-2 Calc No. C-296-01.04

Subject ISFSI FOUNDATION DESIGN Sheet 36 of ____

REV	ORIGINATOR	DATE	IRE	DATE	REV	ORIGINATOR	DATE	IRE	DATE	REV INDICATOR
3	L. Pham	2/26/2007	T. Yee	8/3/07						

CONCRETE DESIGN



$M_u = \frac{q L^2}{2} = \frac{(6.67 - 0.45)(10)^2}{2} = 311$ K-FT

$K_u = \frac{M_u}{bd^2} = \frac{311 \times 12}{12 \times 32^2} = 0.304$ KSI

$\rho = \frac{0.85 \times f'_c}{f_y}\left[1 - \sqrt{1 - \frac{2K_u}{\phi\, 0.85 f'_c}}\right]$ > 0.0033 MIN

$\rho = \frac{0.85 \times 4}{60}\left[1 - \sqrt{1 - \frac{2(0.304}{0.9 \times 0.85 \times 4}}\right] = 0.00594 < 0.018$ MAX

$A_s = \rho bd = 0.00594(12)(32) = 2.28$ IN^2/FT REQUIRED

PROVIDE #11 @ 8" $\therefore A_s = 1.56$ IN$^2 \left(\frac{12}{8}\right) = 2.34$ IN^2

$V_u = (6.67 - 0.45)(10 - 2.67) = 45.6$ K/FT

$\phi V_c = \phi 2\sqrt{f'_c}\, bd = 0.75 \times 2\sqrt{4000}\,(12)(32) = 36.43$ K/FT

$\phi V_s = V_u - \phi V_c = 45.6 - 36.43 = 9.17$ K/FT

$V_s = 9.17 / 0.75 = 12.23$ K/FT

TRY #4 @ 12 IN ON CENTER $A_v = 0.2$ IN$^2 > 50 \frac{bs}{f_y} = \frac{50(12)(12)}{60000} = 0.12$ IN^2 (OK)

$V_s = \frac{A_v f_y d}{s} = \frac{0.2(60)(32)}{12} = 32$ K/FT > 12.23 K/FT (OK)

$\frac{36.43}{(6.67 - 0.45)} = 5.86'$ $\therefore$ AT 5.86' FROM EDGE OF PAD $V_u = 36.43$ K/FT $= \phi V_c$

THUS, PROVIDE #4 STIRRUP @ 12 IN SPACING FROM 4' TO 10' FROM EDGE OF PAD

E&TS DEPARTMENT

CALCULATION SHEET

ECN NO./ ~~A48347~~ GP 5/16/07 PRELIM. CCN NO.	PAGE ____ OF ____
	CCN CONVERSION: CCN NO. CCN -

Project or ECP 061000254-2 Calc No. C-296-01.04

Subject ISFSI FOUNDATION DESIGN Sheet 37 of 37

REV	ORIGINATOR	DATE	IRE	DATE	REV	ORIGINATOR	DATE	IRE	DATE
3	L. Pham	2/26/2007	T. Yee	8/3/07					

REV INDICATOR

TEMPERATURE & SHRINKAGE STEEL IN LONGITUDINAL DIRECTION:

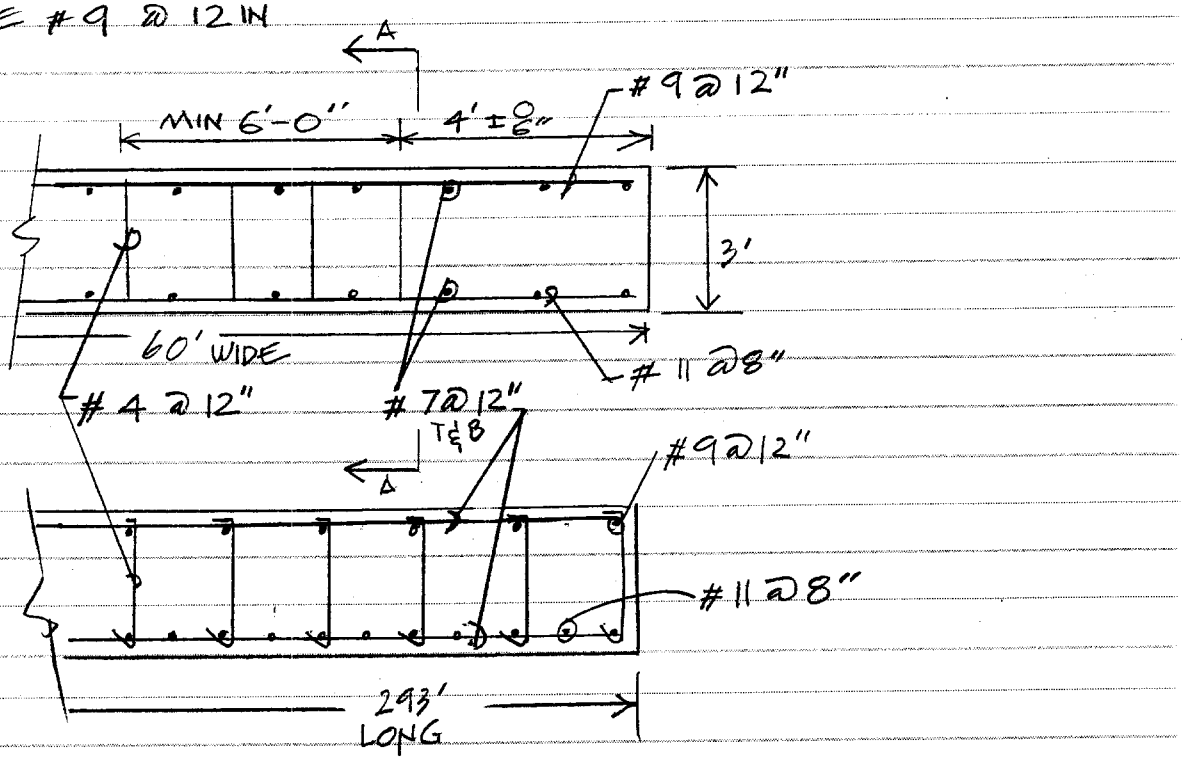
$A_s = 0.0018 \times 36 \times 12 \leq 0.78\ IN^2/FT$

USE #7 @ 12" @ TOP & BOTTOM

$A_{S\,PROV} = 2(0.6) = 1.2\ IN^2/FT > 0.78$ (OK)

TOP LAYER REINFORCEMENT STEEL (HOR DIRECTION)

USE #9 @ 12 IN



SEE A-A